2014

COMPUTATION OF BUOY MOORING CHAIN WEAR

Jonathan P. Benvenuto
University of Rhode Island, jpbenvenuto@my.uri.edu

COMPUTATION OF BUOY MOORING CHAIN WEAR

BY

JONATHAN P. BENVENUTO

A THESIS SUBMITTED IN PARTIAL FULFILLMENT OF THE

REQUIREMENTS FOR THE DEGREE OF

MASTER OF SCIENCE

IN

OCEAN ENGINEERING

UNIVERSITY OF RHODE ISLAND

2014

MASTER OF OCEAN ENGINEERING THESIS

OF

JONATHAN P. BENVENUTO

APPROVED:

Thesis Committee:

Major Professor Jason M. Dahl

Richard Brown

DML Meyer

Harold T. Vincent

Nasser H. Zawia
DEAN OF THE GRADUATE SCHOOL

UNIVERSITY OF RHODE ISLAND
2014

ABSTRACT

The majority of floating AtoN maintained by the U.S. Coast Guard are affixed to the sea bed through use of a chain and a large concrete block also known as a sinker. As a buoy moves through a wave cycle, the buoy chain also moves. This movement causes friction between the links known as interlink wear, but it also results in wear from the surrounding environment. A mooring chain is characterized into three different sections, the riser, chafe and bottom. The chafe section of chain is where most of the wear is found and more often than not, the reason a buoy must be serviced on a regular basis. This thesis will focus on the interlink wear within the chafe section of the chain on a U.S. Coast Guard navigational buoy mooring.

With the total motion of the chain, chain size and material type are known, tribology was used to determine the wear rate of the chain. Since determining the wear rate analytically would be very difficult, empirical based testing was used. An experiment using AISI 1022 hot rolled steel chain, a variable speed motor and various parts was constructed. The device moved the chain in a set vertical direction along a slide resulting in a simulated regular wave motion. Stops at different time intervals were made to measure chain weight and interlink wear. This data was plotted and a curve constant, K, was determined as a function of time which would be used in the program. The experimental results were compared to tabulated and analytical results to find that there was not much variation between each result. Pi parameter regressions were used to help with scaling results to different materials and chain dimensions.

A MATLAB based computer program was written to predict when a buoy mooring would require servicing through a chain wear algorithm which will optimize buoy mooring service intervals and reducing cost to maintain each aid. The program was found to estimate chain wear within 2 percent of observed on in service buoys.

ACKNOWLEDGMENTS

First and foremost, I would like to acknowledge Dr. Jason Dahl for always having the patience and knowledge to help guide me to complete this thesis on time.

I would also like to acknowledge the following people for their role in helping me conquer my feat of this thesis:

- Dr. DML Meyer for helping me with Contact Mechanics and Tribology principles by devoting countless hours of her time both in and out of school to ensure I was set up for success.
- Dr. Richard Brown for providing me with the knowledge and materials so that I could simulate corrosion.
- Dr. Bud Vincent by helping provide equipment and knowledge so that I could successfully complete an experiment.
- Mr. Darrell Milburn for providing assistance and a great deal of reference material from MOORSEL.
- USCG Aids to Navigation Team Bristol, RI for providing me with buoy chain.
- USCGC FRANK DREW and USCGC WILLIAM TATE for their assistance providing me information and technical insight.
- Gail Paolino for her assistance with procurement and paperwork.
- CDR Michael Davanzo for not only being a close mentor and friend, but also teaching me the fundamentals of buoy tending.

- My parents and family for always supporting me through my academic and life challenges.

TABLE OF CONTENTS

LIST OF TABLES

LIST OF FIGURES

CHAPTER 1

INTRODUCTION

1.1 General Overview

Since 1716, the United States Coast Guard (prior to 1939 known as the U.S. Lighthouse Service) has been servicing Aids to Navigation (AtoN). AtoN can be separated into two different forms, fixed and floating. Fixed AtoN are considered to be lighthouses, day boards, ranges, and any other type of a fixed structure that can be used to assist the mariner in navigating a channel; this type of AtoN usually has a very specific location. Floating AtoN are in the form of buoys. These buoys come in all shapes, sizes and colors depending on the intent of their service as well as their geographic location. These buoys are affixed to the ocean bottom through use of a chain and a large weight either in the form of concrete or pyramid shaped steel. Since the sea is never perfectly calm, these buoys tend to move with six degrees of freedom similar to that of a ship. This movement of the buoy will cause the mooring chain to move, this movement causes friction which results in wear. Wear rates of buoy mooring chain vary with the chain and bottom type, corrosion, buoy dimensions and wave spectra induced on the buoy.

The majority of chain wear occurs mostly in the middle section of the chain called the chafe (figure 1.1).

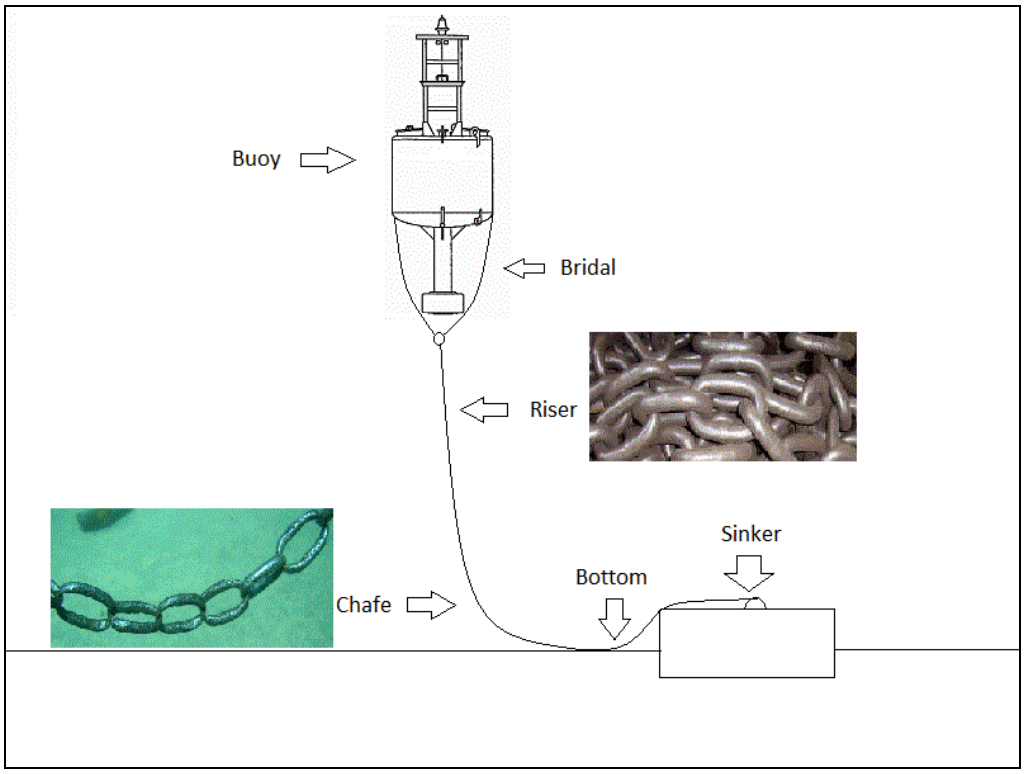

Figure 1.1: Typical USCG Buoy Mooring

More often than not, chain wear is the weak link that determines the buoy mooring's holding power through the test of time, although one cannot discount the holding power of the sinker which can result in the buoy moving out of its specific geographic position, rendering the buoy either a hazard to navigation or causing false interpretation of where the channel is marked. If one looks at the surrounding environment for chain wear, they will find that when chain is placed on a soft bottom such as mud, the wear occurring only happens between the links. When the chain is sitting on bottoms of rock or coral, or on any material that has hardness greater than that of 1022 steel, there will be wear outside of the link. With both interlink and bottom friction, wear rates can be quite high which results in frequent replacement of chain.

The U.S. Coast Guard often uses operational experience, rather than engineering design tools, to select moorings while having the ability to verify the mooring selection with the USCG Aids to Navigation (AtoN) Technical Manual as well as the Mooring Selection computer program, MOORSEL (USCG, 2010). The MOORSEL program provides recommendations as to how a mooring should be designed for a particular geographic area. Although very useful, had some limitations especially with its use with modern computers since it was written in a code used about 20 years ago prior to the computer technology boom. The purpose of selecting the correct mooring is to ensure the buoys remain 'on-station' (figure 1.2) and not become 'off-station' (figure 1.3).

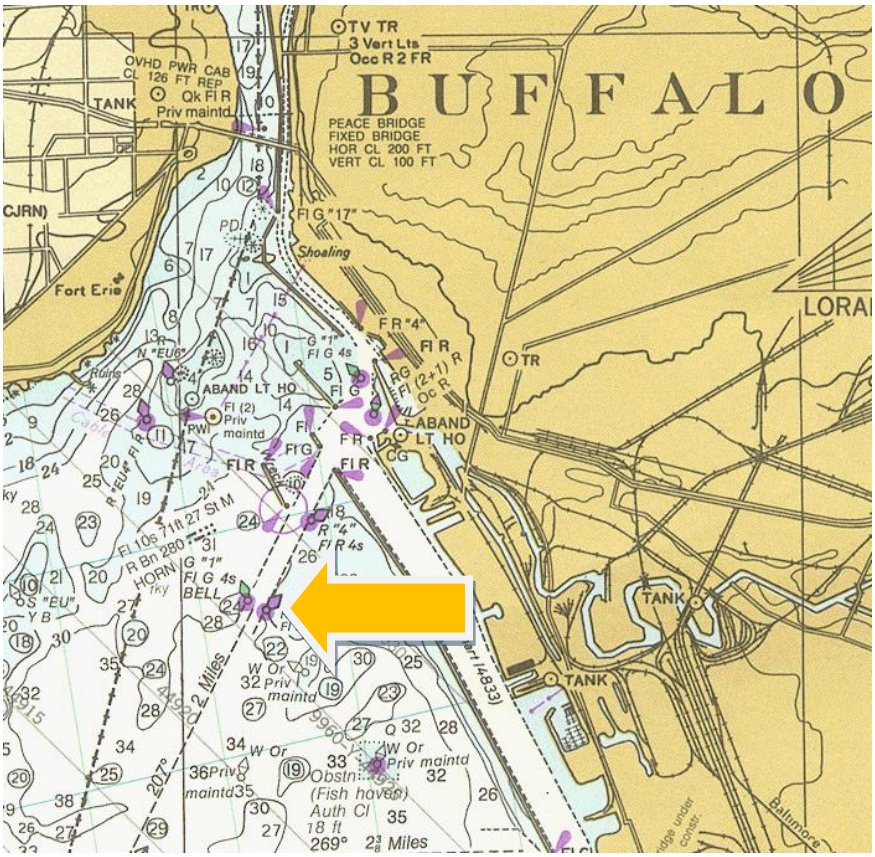

Figure 1.2: On-station. (Library.buffalo.edu)

Figure 2.3: Off-station. (www.hamptonroads.com)

Chain wear was simulated through use of a custom built variable speed chain oscillator that helped to provide accelerated interlink chain wear as well as taking into account corrosion effects on interlink wear. This was completed through use of artificial sea salt as per ASTM D 1141-52 Formula a, Table 1, sec. 4 (i.e. 156 grams of sea salt to 1 gallon of distilled water). The chain oscillation was completed at a set differential height and measurements were taken from a specific link within the chain. With this experiment, the non-dimensional wear coefficient was determined and implemented back into the Archard wear equation where it provides a simulated wear

rate of chain. The equations of motion ultimately provide the total sliding distance due to wave motion over a specific time period which is input into the Archard equation that yields a wear amount.

1.2 Purpose of the Study

Buoy mooring selection has always been a challenge for those who maintain buoys since there are so many variables and options to successfully solve this problem. There was approximately over 200 billion dollars' worth of cargo imported and exported within U.S. waterways in 2013. These waterways contain over 25,000 aids marking them which are maintained by the U.S. Coast Guard; these aids are vital to commerce within the U.S. and must remain in their assigned position. If a chain wears too much, the buoy will break loose upon a surge which exceeds the tensile strength of the steel, resulting in an unmarked or poorly marked channel. Current mooring wear prediction is completed while servicing an aid and is mostly empirical; new aids placed in a new location do not have this data, therefore the service interval is unknown. With a prediction tool, service intervals can be estimated and current service intervals can be lengthened, resulting in decreased costs and allocation of resources elsewhere. The objective of this thesis is to complete a MATLAB based computer algorithm through a set of equations that can be used to provide a prediction of buoy mooring chain wear based on specific user inputs. The equations of motion for a floating cylinder will be integrated with Hertzian theory within contact mechanics to provide a probabilistic estimate of interlink chain wear within a buoy mooring over a user determined length of time. These equations would ideally be

implemented into a user friendly computer program that is compatible with the U.S. Coast Guard workstation.

The data achieved from this study is of the upmost importance since chain wear is one of the major factors requiring moorings to be serviced, the other lesser factors being marine fouling and having the buoy out of position or 'off station.' One goal of this research is to conduct experimental testing to minimize assumptions to yielding more accurate predictions of wear.

CHAPTER 2

REVIEW OF LITERATURE

This chapter presents a review of literature describing previous studies performed and the fundamentals of fluid particle motion in waves. It also describes its link to motion of a cylindrical floating body, the theory of contact mechanics and how it is applied to solve for interlink chain wear.

2.1 Previous studies

There have been previous studies to calculate chain wear within a buoy mooring; these studies often take into account many assumptions that can often yield a wear rate which may only apply to a narrow band of moorings. For example, Fleet Limited Technology has created a Mooring Selection Guide (MSG) computer program at the request of the Canadian Coast Guard (CCG). The information they provided describing the program shows that they did not take into account wave period and amplitude data for each specific location of the buoy nor did it compute probabilistic wave frequencies/heights using wave energy density information. It did however give this information as it relates to water depth; unfortunately the period of a wave is not only dependent on water depth but how it was formed, i.e. wind waves have a short period whereas tidal waves have very long periods. Although it did include an equation (equation 2.1) for computing chain wear by determining the diameter ratio, D_r, of the current diameter compared to the original diameter, D_0. This equation is based on several empirical models that were derived from experimental testing (Dinovitzer, Rene, Silberhorn, & Steele, 1996). The MSG also assumes

characteristics about the soil that could yield an unconservative answer, i.e. mooring in a rocky or coral environment; this would greatly reduce the horizontal resisting force.

$$D_r = \frac{\frac{C_1 D_0 t}{\sqrt{1+t}} + C_2 t^2 + C_3 t}{C_4 Depth + C_5} \tag{2.1}$$

Where: C_1, C_2, C_3, C_4 and C_5 are regression coefficients, t, D_0 and Depth are the duraton of service (in months), new chain nominal diameter (in inches) and water depth (in meters), respectively.

Another study conducted by C. A. Kohler looked into the different material types that made up the chain as an effort to try and determine the cause of buoy chain degradation and how to strengthen corrosion resistance. This study analyzed different materials taking into account corrosive wear, interlink wear and barrel wear. The interlink wear (between the links) and barrel wear (outside the links) were not analyzed in great deal through the study performed by Kohler, therefore the comparative results between the different materials used were achieved empirically. It was found that 4340 steel had the best corrosive wear resistance, followed by 4140 and 8740. This was most likely due to an increase in alloy and Carbon content from 1022 steel (Kohler, 1985). Unfortunately, when applied to budgetary and manfacturing constraints, using any alloyed steel would not be economical, therefore the Coast Guard continues to use 1022 steel within its buoy moorings (Danzik, 1986).

2.2 Fluid, Motion and Waves

Any object that floats in a fluid may be subject to movement within the fluid due to wave action or pressure changes. This concept can be related to Bernoulli's principle as it states when the speed of an object in a fluid increases, the pressure decreases on the object; when the buoy is moving through the water at any rate, the pressure on the hull will vary causing it to react due to the change in force on the hull. In the dynamics of fluid motions, it can be anticipated that force mechanisms can be associated with fluid inertia and weight, viscous stresses and secondary effects such as surface tension. Three primary mechanisms of significant importance are inertial, gravitation and viscous forces (Newman, 1977).

To accurately predict the static and dynamic hydrodynamic loading and properties on an offshore floating structure, there are a few methods used such as Boundary Element Method (BEM), Finite Element Method (FEM) and analytical methods. The analytical method for a simple floating cylinder is the most efficient and accurate method sufficient for describing buoy motions, but for more complex structures this would be very difficult to complete therefore yielding to BEM and/or FEM (Ghadimi, Bandari, & Rostami, 2012).

The fluid motion equations used throughout this study assume that sea water is incompressible, inviscid (or *ideal fluid*) and the fluid motion is irrotational (vorticity vector is zero everywhere in the fluid). These conditions satisfy the solution of the following Laplace equation (Faltinsen, 1990):

$$\frac{\partial^2 \emptyset}{\partial x^2} + \frac{\partial^2 \emptyset}{\partial y^2} + \frac{\partial^2 \emptyset}{\partial z^2} = 0 \qquad (2.2)$$

Other assumptions one must consider for this problem are surface tension at air-water interface is negligible and water is at a constant density and temperature (Finnegan, Meere, & Goggins, 2011).

One must also consider the kinematic boundary condition (the velocity of fluid on the boundary) assumption that there is no permeability normal to the body's surface since the steel makeup of the buoy is an impermeable surface. The kinematic boundary condition (equation 2.3) fluid flowing normal to the bodies velocity is equal to the body's velocity, it is also assumed to be equal to the tangential flow of the velocity, if it exists (Faltinsen, 1990).

The dynamic free-surface boundary condition (forces on the boundary) equation 2.3a, assumes that the water pressure is equal to a constant atmospheric pressure on the free surface (Newman, 1977). Free surface conditions are often very complicated and difficult to model; for simplification and to allow for linear analysis, the free surface boundary condition may be linearized. Since we are looking to develop a simple, quick tool for analysis of a simple system over long periods of time, the linearization assumption significantly simplifies the computation to significantly reduce computational time.

In order to solve Laplaces' equation, one must identify the physical boundary conditions such as the linearized free surface boundary conditions in the following equations (Ghadimi, Bandari, & Rostami, 2012):

$$\frac{\partial \vartheta}{\partial t} = \frac{\partial \emptyset}{\partial z} \quad \text{at z = d (kinematic condition)} \tag{2.3}$$

$$g\vartheta + \frac{\partial \emptyset}{\partial t} = 0 \quad \text{at z = d (dynamic condition)} \qquad (2.3a)$$

$$\frac{\partial^2 \emptyset}{\partial t^2} + g\frac{\partial \emptyset}{\partial z} = 0 \;\; at\; z = d \qquad (2.4)$$

These boundary conditions will be used as the basis for describing linear wave motion. Equation 2.2 describes the motion of the fluid being irrotational (velocity as a gradient of a scalar, Φ) as well as the fluid being incompressible (Newman, 1977). Equation 2.4 is developed by combining equations 2.3 and 2.3a. The linearized movement of the particles on the free surface (or free surface boundary condition) can be described by using equation 2.4. The linear free surface condition will depend on the presence of any current, in equations 2.3 and 2.3a we assume the current is zero as linear theory states the velocity potential is proportional to the wave amplitude (Faltinsen, 1990).

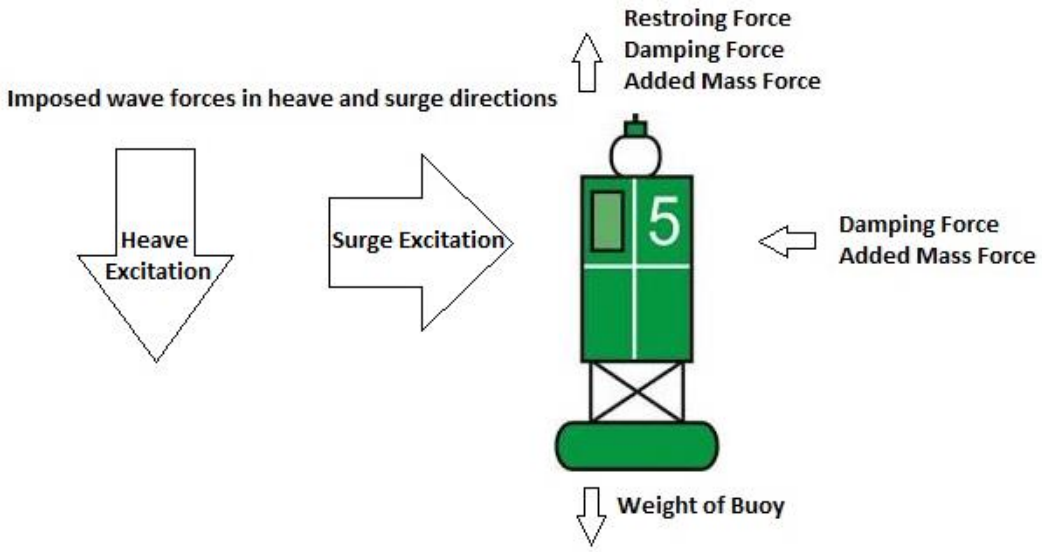

Figure 2.1: Free body diagram of forces acting on a buoy that will be modeled.

An analytical way of describing how a floating object reacts when a regular wave is imposed on it would be to use the free surface boundary equation (2.4) in conjunction with the Laplace equation (2.2) and bottom boundary condition to develop the exciting forces (2.4c) imposed on the cylinder in heave through calculation of both interior and exterior solutions around the cylinder (Ghadimi, Bandari, & Rostami, 2012).

This study used more of an analytical method by first taking the sum of the external forces for a spring mass within the time domain as seen in equation 2.4a.

$$F_j(t) = \sum_{k=1}^{6} M_{jk}\ddot{n}_k + B_{jk}\dot{n}_k + C_{jk}n_k \quad j = 1,2,....6 \tag{2.4a}$$

$$F_j(t) = F_{Ij}(t) + F_{Dj}(t) + F_{Rj}(t) \quad j = 1,2,....6 \tag{2.4b}$$

$$F_{Ej}(t) = F_{Ij}(t) + F_{Dj}(t) \quad j = 1,2,....6 \tag{2.4c}$$

Where:

F_{Ij} = Incident (Froude-Krylov) Forces

F_{Dj} = Diffraction forces

F_{Rj} = Radiation forces

Equation 2.4a assumes that motions are linear and harmonic, neglecting quadratic terms and linearizing assuming only small amplitude motions (Bonfiglio, Brizzolara, & Chryssostomidis, 2012). Without being immersed in a fluid, the structural equation for motion, 2.4a would apply. The force equilibrium is shown in 2.4b and the

breakdown of the excitation forces (F_{Ej}) are shown in 2.4c. Since the buoy is surrounded by fluid this introduces added mass (F_{Rj}), damping and restoring forces which are provided by the fluid. These forces alter the effective structural properties of the buoy yielding equation 2.4d.

$$F_{Ej}(t) = \sum_{k=1}^{6} [(M_{jk} + A_{jk})\ddot{n}_k + B_{jk}\dot{n}_k + C_{jk}n_k] \quad j = 1,2,\ldots.6 \tag{2.4d}$$

For the purposes of this study, this equation is best utilized in the frequency domain vice the time domain since the wave spectra imposed onto these equations will be defined in the frequency domain, therefore the exciting force in heave in the frequency domain will be equation 2.5 (Bonfiglio, Brizzolara, & Chryssostomidis, 2012). The transfer function (solved for H_j, amplitude of the response) used to generally describe the motion of a floating cylinder when set equation to the spring mass equation is the Fourier transform of equation 2.4d:

$$H_j = \frac{F_{EX_j}}{\left(-\omega_e{}^2(\Delta + A_{jk}) + i\omega_e B_{jk} + C_{jk}\right)} \quad \text{j =1,3} \tag{2.5}$$

The entire left hand side of the equation as seen in equation 2.5 is known as the radiation force of the floating body (Lewis, 1989). The right hand side of equation 2.5 is not zero as it would be in a spring-mass damped system with no external forces, therefore the motion will not diminish over time. These external forces also known as exciting forces are normally divided into two parts, the Froude-Krylov (or incident) and diffraction excitations. If the wavelength of the incoming wave is long, then the

Froude-Krylov forces dominate whereas if the incoming wave wavelength is short, the diffraction force becomes significant (Lewis, 1989). When describing the motion of a floating body, the excitation force appears to be the most varied and dependent on the geometry of the body that the force in placed upon. To help determine this force on irregular shaped bodies, strip theory is often used; breaking down the geometry into thin strips describing one dimension of the body and integrating over another dimension therefore describing the geometry of the surface at which the forces are acting upon.

Now that we have an idea of the general form of body motions, one needs to consider the six degrees of freedom motion; surge, sway, heave, roll, pitch and yaw. In this thesis, the surge and heave motions will only be analyzed (equations 2.3b and 2.5) as they appear from visual inspection to be the two motions that have the greatest effect on chain wear within the mooring. This assumption does not take into account the coupling with any other forces from the remaining four degrees of freedom which could yield an inaccurate heave or surge response. Heave is about equal to the wave height for most buoys but often long slender bodies such as a spar buoy may not follow that rule in different wave heights, therefore we need to calculate excitation forces on the body (Paul, Irish, Gobat, & Grosenbaugh, 2007). The excitation force equation varies based upon which motion direction is being described whereas the radiation portion of the equations maintains the same form.

For the surge condition, this method was used since there was enough data to support use of the equations yielded. By computing and combining both interior and exterior solutions as well as using equations 2.2 through 2.4 in the frequency domain,

equation 2.5a was determined as the excitation force for the surge motion of a cylindrical body floating in water.

$$\hat{F}_{1,ext} = -\frac{2\pi i\rho gAa}{k_0}\{J_1(k_0a) - J_1'(k_0a)\frac{H_1^{(1)}(k_0a)}{H_1^{(1)\prime}(k_0a)}\}(1 - e^{-k_0b}) \quad (2.5a)$$

Where:

k_0 is the wave number

ρ is the density of water

g is gravity

A is amplitude of the wave

a is radius of the cylinder

b is draft of the cylinder

The excitation force in surge will be placed equal to the spring mass equations as seen in linearized equation 2.5 to determine the motion of the buoy in the surge direction. The detailed equation(s) used to describe the excitation force in the heave direction used in this study is (Lewis, 1989):

$$F_{EX_3} = -\delta \int_L e^{ikx} e^{-kT(x)} [c_{33} - \omega_0(\omega_e a_{33} - ib_{33})]dx \quad (2.7)$$

$$\omega_e = \omega + \omega^2 \frac{g}{U_0} \quad (2.8)$$

Where:

a_{33} is the sectional heave added mass

b_{33} is the sectional heave damping

c_{33} is the sectional restoring force
δ is the incident wave amplitude
$T(x)$ is the mean section draft
ω_e is the frequency of wave encounter

The sectional heave added mass, a_{33}, and sectional heave damping, b_{33}, for this particular problem were first determined from experimental data from Vugts (1968) performed with rectangular cylinders (Newman, Marine Hydrodynamics, 1977).

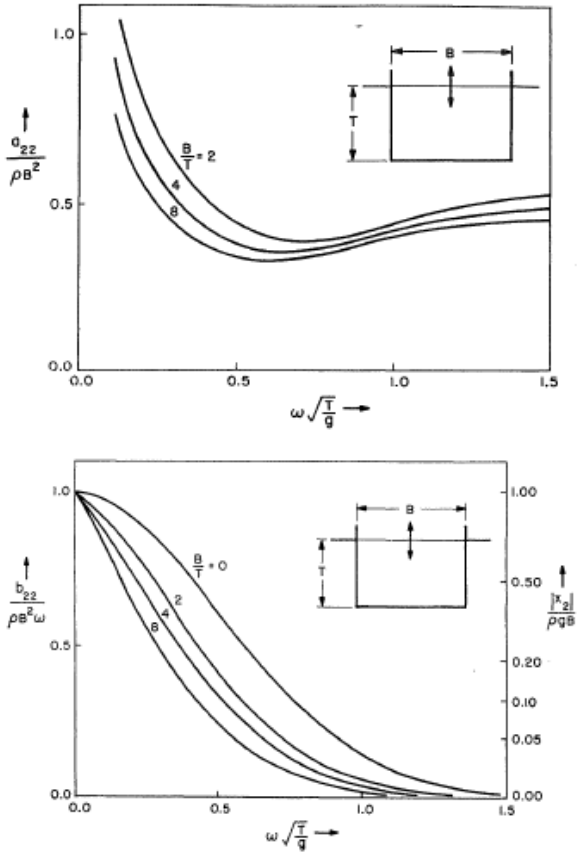

Figure 2.1a: Added mass and damping coefficients (Newman, Marine Hydrodynamics, 1977).

Although this does not exactly model the results of a cylindrical cylinder, it can be used to achieve a close approximation. To get a better approximation of the excitation

force in the heave direction, the added mass and damping coefficients were used as seen in figure(s) 2.2 and 2.3 (Bonfiglio, Brizzolara, & Chryssostomidis, 2012).

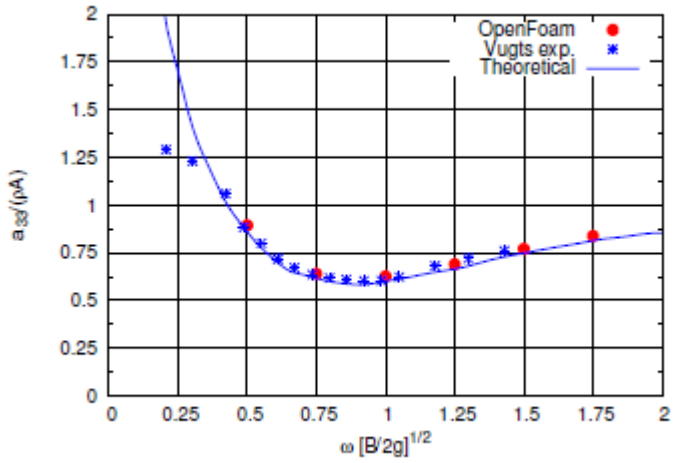

Figure 2.2: Added mass coefficient for a circular section. (Bonfiglio, Brizzolara, & Chryssostomidis, 2012)

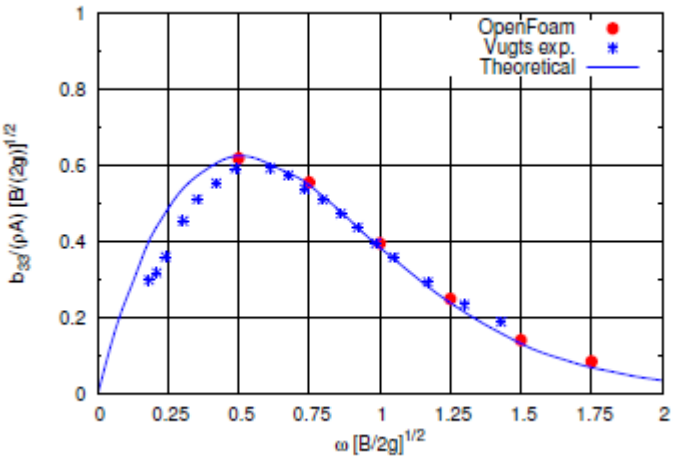

Figure 2.3: Damping coefficient for circular section. (Bonfiglio, Brizzolara, & Chryssostomidis, 2012)

Once the excitation forces are computed, they can be placed back into the general transfer function (equation 2.5) and where '$H_{1,3}$' will be solved. When a *regular* wave (shape of a sine wave) of a specific amplitude and frequency is placed upon the structure, the transfer function will directly describe the motion of the body.

The excitation force is a function of wave amplitude and frequency while the transfer function is only a function of frequency. The transfer function is made up of four different dynamic forces; the body-induced pressure force, the body-mass force, the hydrostatic force and the Froude-Krylov force (Newman, 1977). Once the transfer function is known, the movement of a floating body can be determined when a regular wave is induced on it.

Unfortunately, large bodies of water do not produce all of the same size waves with the same frequency from the same direction; therefore this wave action is often described through use of a probabilistic wave spectra developed through experiments. The spectra concept dates back to Sir Isaac Newton who discovered the spectrum of colors in sunlight; when describing waves, the spectra of various regular sine waves with different amplitudes and frequencies, also known as wavelets, are all added together to give a superposed wave, or the wave that is normally seen when in the actual environment. The energy distribution of these wavelets is plotted against frequency to give a direction independent frequency spectrum; if direction dependent, then known as a directional wave spectrum (Goda, 2010). A continuous spectrum of these wavelets is known as a frequency spectral density function or wave energy density spectrum with units of m^2s. The wave energy density spectrum (see figure 2.4) is a probabilistic curve developed through many years of wave observations; there are a few different wave energy density spectrums developed for different bodies of water, i.e. Joint North Sea Wave Observation Project (JONSWAP) was developed using wave data from the North Sea.

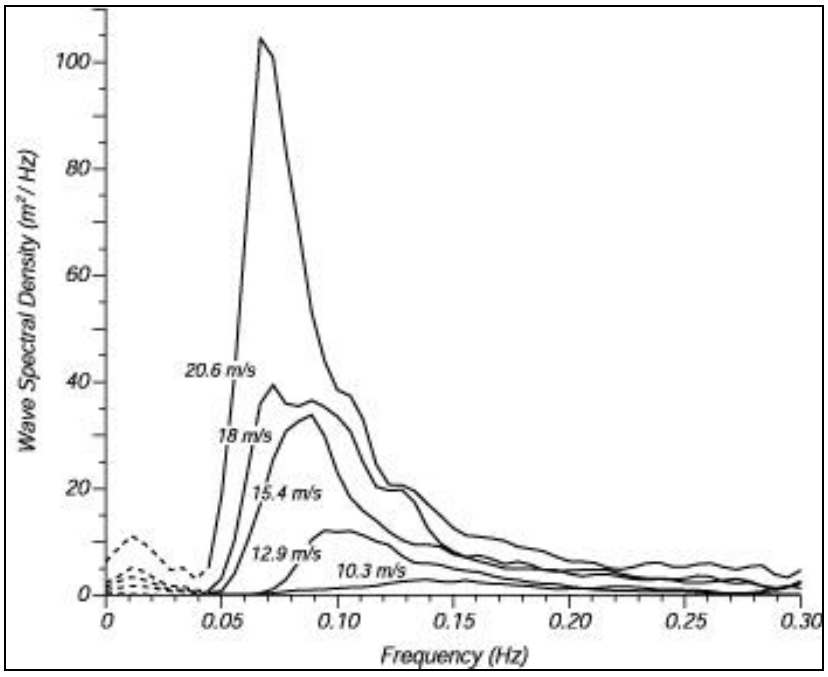

Figure 2.4: P-M wave spectrum for different wind speeds (www.wikiwaves.org)

Other wave energy density spectrums include the Pierson-Moskowitz data that was developed through empirical observations in the North Atlantic or the modified Bretschneider-Mitsuyasu spectrum that is used to describe a frequency spectrum of wind waves (Goda, 2010). The sea spectrum that is highly desired (see figure 2.4) is the JONSWAP due to its wide acceptance as a frequency spectrum that covers most wave forms.

$$S(f) = \beta_J H_{1/3}^2 T_p^{-4} f^{-5} \exp[-1.25(T_p f)^{-4}] \gamma^{\exp[-(T_p f - 1)^2/2\sigma^2]},$$

in which

$$\beta_J = \frac{0.0624}{0.230 + 0.0336\gamma - 0.185(1.9 + \gamma)^{-1}} [1.094 - 0.01915 \ln \gamma],$$

$$T_p \simeq T_{1/3}/[1 - 0.132(\gamma + 0.2)^{-0.559}],$$

$$\sigma = \begin{cases} \sigma_a : f \leq f_p, \\ \sigma_b : f \geq f_p, \end{cases}$$

$$\gamma = 1 \sim 7 \text{ (mean of 3.3)}, \ \sigma_a \simeq 0.07, \ \sigma_b \simeq 0.09.$$

Figure 2.5: JONSWAP equations used (Goda, 2010)

Where: *S(f)* is the JONSWAP sea spectrum

f = frequency of the wave

f_p = frequency at spectral peak

γ = peak enhancement factor

If required to produce a more accurate result for different geographic areas such as large bays or the Great Lakes, other sea spectra can be implemented with not much difficulty. The purpose of the sea spectra is to provide a close probabilistic estimate given specific geographic wave characteristics, i.e. significant wave height and period, to shape the sea spectrum so that it best reflects what is seen at that specific location. The sea spectra will then be combined with the transfer function to output a total body motion in an *irregular* sea and therefore provide a much more accurate estimate on the motions of the floating body.

2.3 Resultant Buoy Motion: Heave and Surge

Once the motions required to solve the problem have been identified, analysis of how the floating object moves in those directions can occur; in this case heave and

surge have been identified as key forces in determining buoy chain wear. Since the motion of a buoy within a regular wave set (transfer function) and the frequency spectrum of sea waves are known, both pieces need to be synergized to yield the total heave and surge motion of the buoy given a variation of wave frequencies. The variance of the response over a range of frequencies can be determined using the following equation (Faltinsen, 1990):

$$\sigma_r^2 = \int_0^\infty S(\omega)|H(\omega)|^2 d\omega \tag{2.11}$$

The variance equation can then be used to determine the response of the buoy in an irregular seaway, this is also known as the Response Amplitude Operator or RAO.

With the RAO known, it is then used to determine the root mean squared response for a specific frequency at time 't' and plotted as response versus time as seen in equation 2.12.

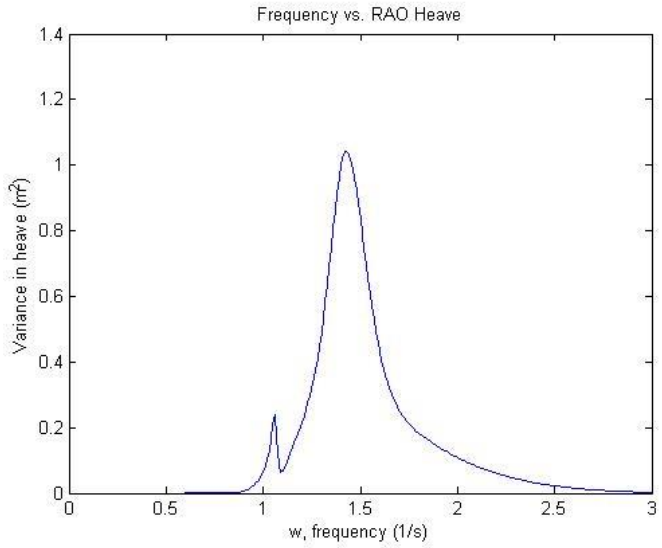

Figure 2.5a: Example of an RAO in heave.

$$R_T = \sum_n \sqrt{2}\sqrt{\sigma_n}\, Cos(\omega_n t + \varphi_n) \tag{2.12}$$

Where: φ is the random phase at which the response is calculated, separating it from the other responses.

The response, R_T, of the buoy motion in the heave direction correlates with changes in water depth seen by a buoy while the response in the surge direction correlates how the buoy moves in the horizontal direction due to the wave action. In the horizontal or surge direction, since the buoy is not moving over the ground, the water passing by the buoy will be induced via current. The current may be caused by wind, tidal or natural river forces; all of which will have the same effect on the buoy below the waterline. The coefficient of drag on a cylinder is used to help determine the horizontal drag force on a buoy; this drag force varies as a function of Reynolds number as seen in figure 2.6. Drag forces are merged with surged forces within the algorithm when determining total horizontal forces resulting from buoy motion. Therefore the Reynolds number (equation 2.13), a non-dimensional quantity used to determine certain flow characteristics of a fluid, must be determined, 'U' representing the fluid speed, 'd' the diameter of the cylinder and 'v' the kinematic viscosity.

$$Re = \frac{Ud}{v} \tag{2.13}$$

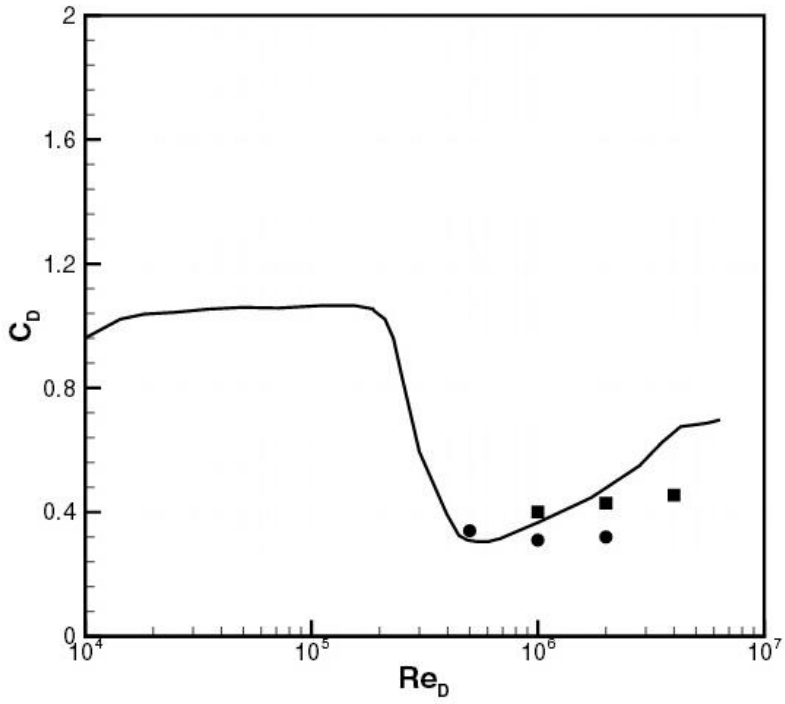

Figure 2.6: Cd vs. Re (Catalano, Wang, Iaccarino, & Moin, 2003)

In conjunction with the current force, one can take the second derivative of the heave response to yield the buoy acceleration in the horizontal direction as a function of frequency. Using Newton's second law and multiplying the acceleration of the body in the horizontal direction by the mass the force in the x-direction due to irregular sea spectra can be determined. The force due to sea spectra summed with the current force will give the total force in the surge direction seen by the buoy, assuming wind effects are negligible.

With the horizontal and vertical forces of the buoy, the vertical and horizontal components of chain tension where the buoy attaches to the chain can be calculated. Current has an effect on both the buoy as well as the tension on the chain. In this study, the current is assumed to be a constant throughout the entire depth of the mooring but actual tests show the current varies non-linearly with depth. The drag

coefficient of U.S. Coast Guard buoy chain what determined to be approximately 1.2 for speeds less than 4 knots (Ross, 1974). It was inconclusive from the data on how exactly the drag coefficient varied with Reynolds number; this will be used as a conservative value to calculate horizontal drag on the mooring. It is hard to conclude how the Sea tests have shown that alternating tension are proportional to chain mass and added mass at low sea states and at high sea states drag grows quadraticly with wave height; another significant source of chain tension (Paul, Irish, Gobat, & Grosenbaugh, 2007). The horizontal and vertical components of tension are what will determine the size of anchor to keep the buoy in one specific geographic location. Many times in a catenary chain system, the submerged weight of the chain itself will hold the buoy in one location. This is accomplished since the vertical tension in the chain is not large enough to support the full weight of the chain; therefore it rests on the bottom and provides resistance. The equations used to describe this catenary shape are seen in equations 2.13a and 2.13b as well as figure 2.6a (Irvine, 1981).

$$l = \frac{HL_0}{EA} + \frac{HL_0}{W}\left[sinh^{-1}\left(\frac{V}{H}\right) - sinh^{-1}\left(\frac{V-W}{H}\right)\right] \quad (2.13a)$$

$$h = \frac{WL_0}{EA}\left(\frac{V}{W} - \frac{1}{2}\right) + \frac{HL_0}{W}\left[\left\{1 + \left(\frac{V}{H}\right)^2\right\}^{1/2} - \left\{1 + \left(\frac{V-W}{H}\right)^2\right\}^{1/2}\right] \quad (2.13b)$$

Where: H is horizontal tension

V is vertical tension

L_0 is length along the chain

W is the weight of the chain per unit

E is the elastic modulus of the material

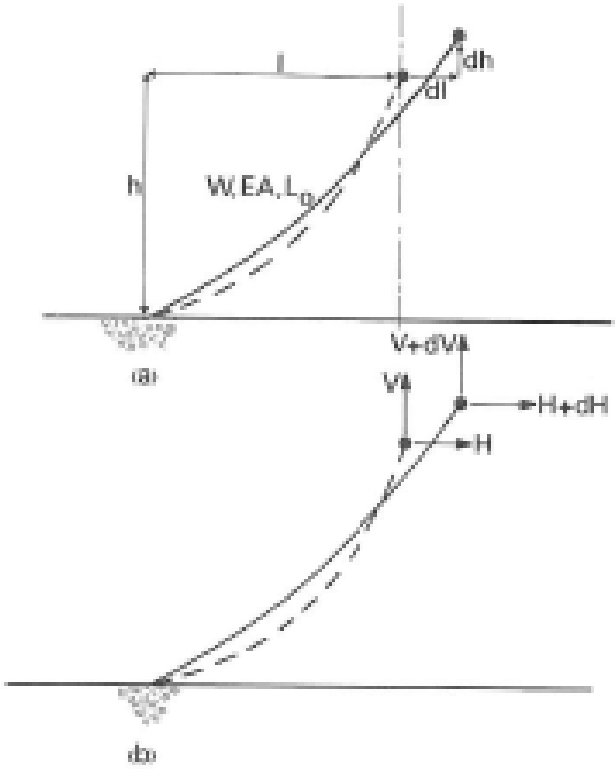

Figure 2.6a: Definition diagrams for a guy with appreciable sag (Irvine, 1981).

Equations 2.13a and 2.13b were used by discretizing the chain into a specific number of parts and applying both equations to each part taking into account the change in weight of the chain. These equations can be used in a quasi-static model to predict the dynamic motion of the catenary.

The determination of motion and forces within a mooring system is critical to discover how the chain will be moving along with the tension that will be experience within the chain assuming it is anchored sufficiently to the bottom of the sea bed.

2.4 Wear

Just about every piece of mechanical equipment has some version of wear; this wear and the tolerances which it can operate in will determine how long of a service life it has. Chain wear is a key failure mechanism when looking closely at catenary moorings used by the Coast Guard. Chain catenary moorings are limited by depth depending on the chain and buoy size but can used in depths up to 900 meters (Paul, Irish, Gobat, & Grosenbaugh, 2007). There have been many studies talking about wear of materials and motions of floating bodies, none that have yielded an analytical predication tool for mooring chain wear. This study will look at the tribological attributes of interlink chain wear focusing in on three encompassing wear mechanisms: adhesive wear, abrasive wear and corrosive wear. Adhesive wear is the state at which two materials have significant traction on one another that may cause a local molecular failure; this failure results in the separation of debris from both materials. Abrasive wear will simulate the act of cutting, fatigue failure and material transfer due to the surrounding environmental conditions or the shape and hardness of the material that it is rubbing against. Corrosive wear is the loss of material due to the chemical interactions occurring within the surrounding environment (Meng & Ludema, 1995).

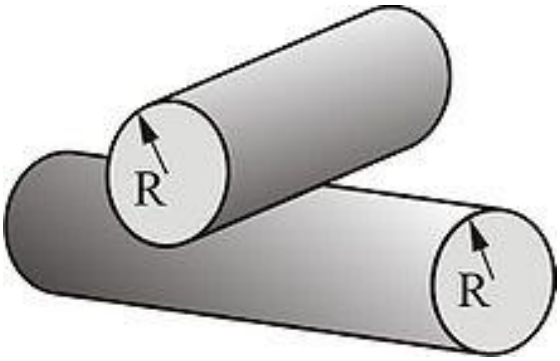

Figure 2.6b: Crossed cylinders. (http://en.academic.ru/)

In the case of two chain links contacting each other, it is assumed that this contact will be simulated as two cylinders orthogonal to each other as seen in figure 2.6b. Since the cylinders are orthogonal, according to Hertzian theory the point of contact can be simulated as two spheres contacting each other, i.e. a circular point contact. A simplified set of Hertz elastic stress formulae used in determining stress components are shown in equations 2.14-2.20 (Johnson, 1985).

$$E^* \equiv \left(\frac{1-\nu_1^2}{E_1} + \frac{1-\nu_2^2}{E_2} \right)^{-1} \tag{2.14}$$

$$R \equiv (1/R_1 + 1/R_2)^{-1} \tag{2.15}$$

Radius of contact circle:

$$a = \left(\frac{3PR}{4E^*} \right)^{1/3}$$

Max. contact pressure: (2.16)

$$p_0 = \left(\frac{3P}{2\pi a^2} \right) = \left(\frac{6PE^{*2}}{\pi^3 R^2} \right)^{1/3} \tag{2.17}$$

Approach of distant points:

$$\delta = \frac{a^2}{R} = \left(\frac{9}{16} \frac{P^2}{RE^{*2}} \right)^{1/3} \tag{2.18}$$

Max. shear stress:

$$\tau_1 = 0.31 p_0 \text{ at } r = 0, \quad z = 0.48a \tag{2.19}$$

Max. tensile stress:

$$\sigma_r = \tfrac{1}{3}(1 - 2\nu)p_0 \text{ at } r = a, \quad z = 0 \tag{2.20}$$

Where: ν = Poisson's Ratio

E = modulus of elasticity

R = radius of body

P = load

Hertizian theory also makes a few other assumptions such as the material must be linearly elastic & isotropic (LEI solid) and the contact must be non-adhesive.

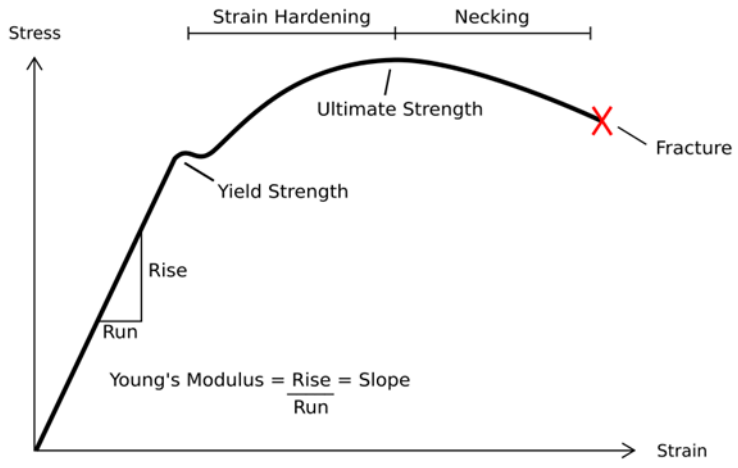

Figure 2.6c: Example of a linear-elastic solid.

Using these assumptions greatly simplifies the contact problem but the uncertainty in the solution is also increased. Johnson, Kendall, and Roberts also have known solutions for problems but it assumes the contact surface is adhesive; the solution for

this type of contact can be determined fairly simply through a further iteration of the problem.

Before a wear computation can be made, one must consider whether or not wear is occurring on the surface that is being analyzed. Von Mises yield criterion is made into what is called Von Mises stress (equation 2.21), a scalar value of stress that is computed from internal stresses in a material (Popov).

$$\sigma_V = \frac{1}{\sqrt{2}}\left[\left(\sigma_{xx}-\sigma_{yy}\right)^2+\left(\sigma_{xx}-\sigma_{zz}\right)^2+\left(\sigma_{zz}-\sigma_{yy}\right)^2+6\left(\tau_{xy}^2+\tau_{xz}^2+\tau_{yz}^2\right)\right]^{1/2} \quad (2.21)$$

If the Von Mises stress exceeds the yield stress, $\sigma_{y,}$ for the material, deformations will occur in the material. Figure 2.7 shows that assuming Hertizan conditions and circular contacts, there will be yielding when two chains are loaded even if only with five Newton's of force.

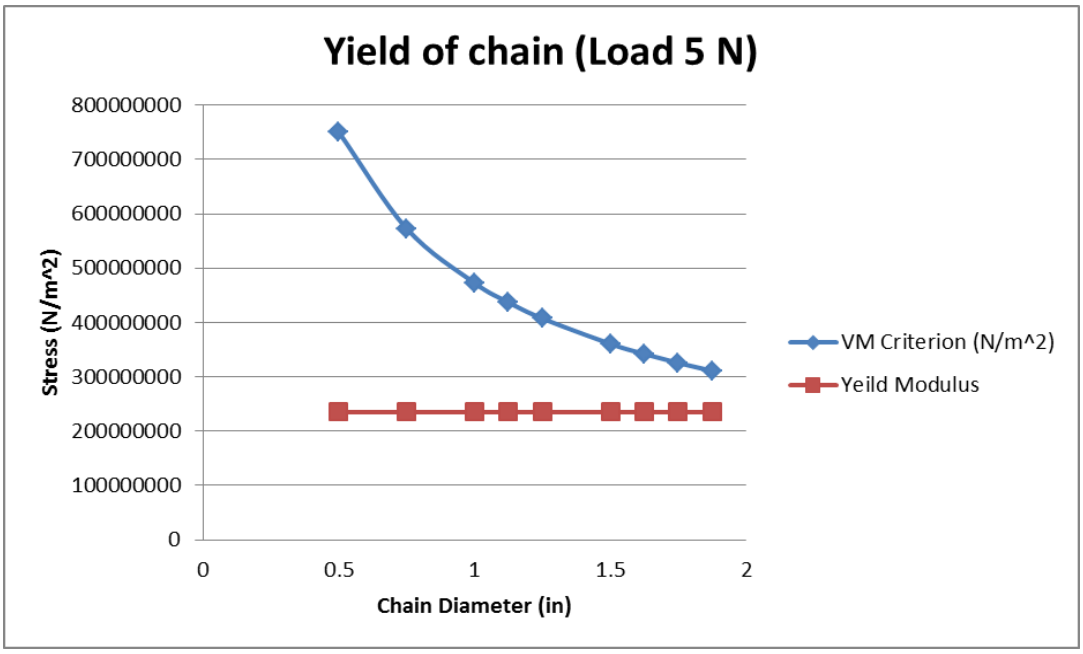

Figure 2.7: Von Mises stress and Yield Modulus

The stress components that make up the Von Mises stress in this case are known as internal stresses within a Hertzian contact, equations 2.22-2.27. Each of these equations describes the influence of a single, vertical force acting at the origin (Popov, 2010). These equations are used to determine whether or not wear is going to occur at the surface by calculating the stress and shear.

$$\sigma_{xx} = \frac{F}{2\pi}\left[-3\frac{x^2 z}{r^5} + (1-2\nu)\left(\frac{x^2(2r+z)}{r^3(r+z)^2} - \frac{r^2 - rz - z^2}{r^3(r+z))}\right)\right] \tag{2.22}$$

$$\sigma_{yy} = \frac{F}{2\pi}\left[-3\frac{y^2 z}{r^5} + (1-2\nu)\left(\frac{y^2(2r+z)}{r^3(r+z)^2} - \frac{r^2 - rz - z^2}{r^3(r+z))}\right)\right] \tag{2.23}$$

$$\sigma_{zz} = -\frac{3F}{2\pi}\frac{z^3}{r^5} \tag{2.24}$$

$$\tau_{xy} = \frac{F}{2\pi}\left[-3\frac{xyz}{r^5} + (1-2\nu)\frac{xy(2r+z)}{r^3(r+z)^2}\right] \tag{2.25}$$

$$\tau_{yz} = \frac{3F}{2\pi}\frac{yz^2}{r^5} \tag{2.26}$$

$$\tau_{xz} = \frac{3F}{2\pi}\frac{xz^2}{r^5} \tag{2.27}$$

In contact mechanics, a common equation used to describe wear is through use of the Archard wear equation (equation 2.28). This equation is often the simplest of most wear equations but it makes many assumptions to simplify its calculation. Both materials must be considered as linear elastic, isotropic, and non-adhesive contact is assumed (Johnson, 1985).

$$w = \frac{KFs}{H} \tag{2.28}$$

Where:

K is the non-dimensional wear coefficient

H is the material hardness measured in units of force per area

s is the total sliding distance of the material

F is the force normal to the wear

The specific wear rate or dimensional wear coefficient, K/H, is usually quoted in units of $mm^3N^{-1}m^{-1}$ and is an empirically derived value varied between two materials and their environment (Williams, 1999). Normal force between the two materials is represented by 'F' and the total sliding distance is 's.' Total material volume removed is represented by 'w.' The Archard wear equation is only a starting point, it assumes that particles are removed from the surface in a uniform manner and the surface maintains its same general shape, a phenomenon that proves this assumption void can be seen in figure 2.7a (Thompson & Thompson, 2006). It is believed this chain wear can be predicted to a certain degree through analytical analysis validating results with empirical data recorded by buoy servicing units.

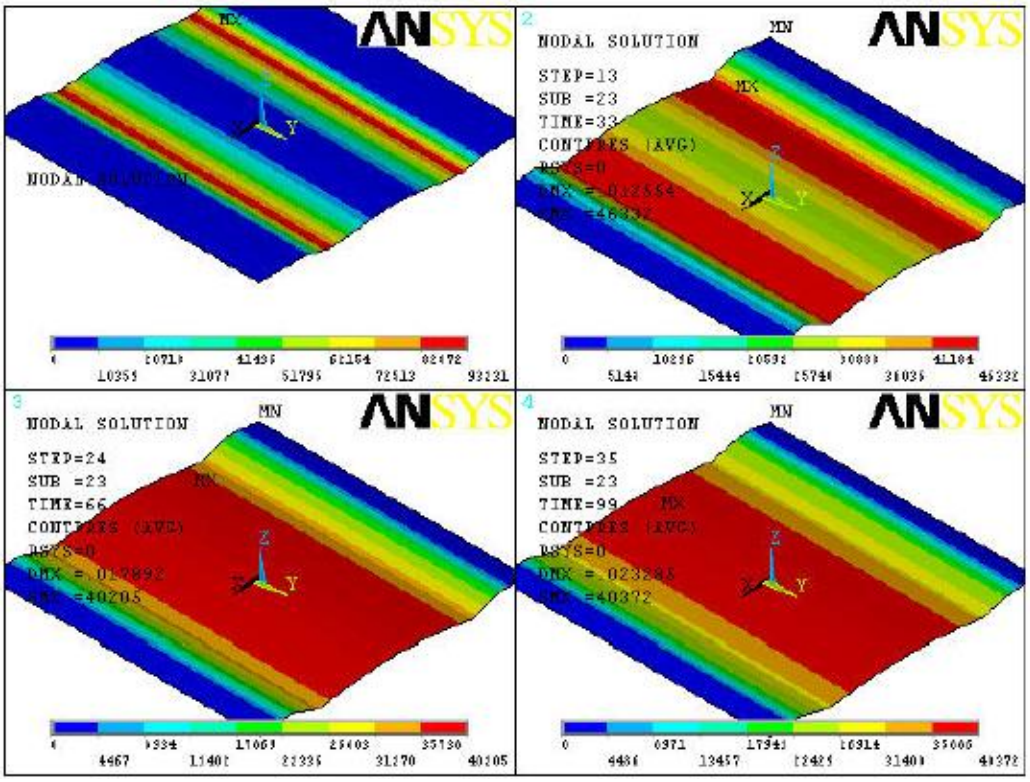

Figure 2.7a: Contact pressure at different times and different amount of wear (Thompson & Thompson, 2006)

Since the chain starts out as a point (1-D) or circular (2-D) contact, the wear will most definitely occur even under the smallest load (figure 2.7), but as the contact point begins to wear, the surface area greatly increases distributing the load and helping to reduce the wear rate. The change in surface volume for two cylinders orthogonally is assumed to be two spheres following Hertzian theory that two cylinders orthogonally form a point contact in this 1-D system (Johnson, 1985). Assuming both spheres are wearing at the same rate, this wear geometry can be modeled as a spherical cap. An expression for 'd' the distance from the center of the chain to the edge of the removed spherical cap is shown in equation 2.29. This expression is used to describe the diameter of the chain that has been worn down (see

figure 2.8); the volume in the expression is half of the total wear volume per contact as there are two spherical caps that are worn per connection (Spherical cap, 2011).

$$d = \frac{\sqrt[3]{\sqrt{3}\sqrt{3V^2 - 4\pi r^3 V} + 2\pi r^3 - 3V}}{\sqrt[3]{2\pi}} + \frac{\sqrt[3]{2\pi}\, r^2}{\sqrt[3]{\sqrt{3}\sqrt{3V^2 - 4\pi r^3 V} + 2\pi r^3 - 3V}} \quad (2.29)$$

Knowing the remaining diameter left on the chain will help in determining whether or not a chain will be suitable for withstanding extreme conditions and requires replacement. The remaining area can be determined through use of geometry based equations. Looking at figure 2.8, the darker region on the bottom half of the sphere is what we are interested in knowing the cross-sectional area of; this is also shown in figure 2.9 by the area not shaded in.

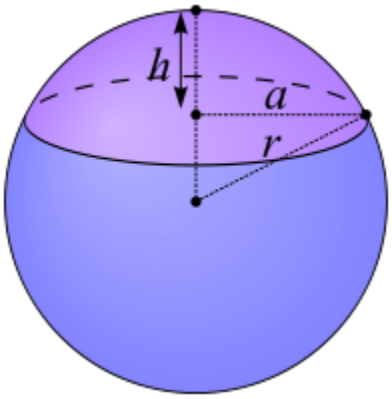

Figure 2.8: Spherical Cap (Spherical cap, 2011)

Since we know the worn depth d, where d=h, we can determine the radius of the cut off semicircle known as ‘a’ in figure 2.8 and ‘c/2’ in figure 2.9 (equation 2.30).

$$a = \frac{c}{2} = \sqrt{-d(d - 2r)} \quad (2.30)$$

Once ‘a’ or ‘c/2’ are known, Θ can be solved for in equation 2.31 which will be used directly in equation 2.32 to determine an estimate of the cross sectional area remaining noted in the unshaded section of figure 2.9.

$$\theta = \cos^{-1}\left(1 - \frac{2a^2}{r^2}\right) \tag{2.31}$$

$$As = \frac{r^2}{2}(\theta - \sin\theta) \tag{2.32}$$

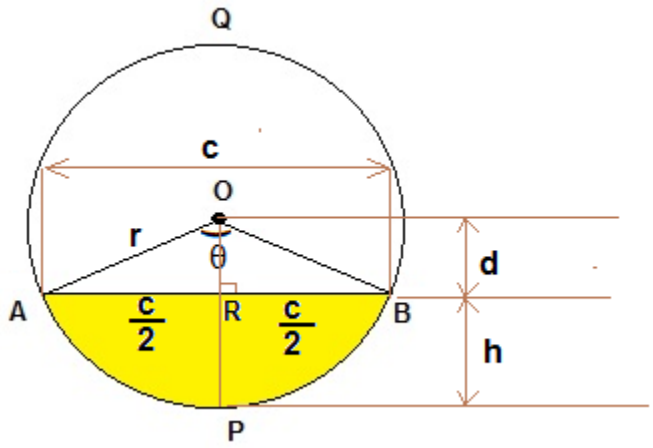

Figure 2.9: Circle Segement (Segment of a Circle)

The total area of steel remaining can then be multiplied by the ultimate and yield tensile strengths of the material to determine the load at which the link will yield and break, respectively. Ultimate and yield tensile strengths for 1022 steel are 61,600 and 34,100 psi, respectively.

The hardness of geologic materials are measured on the Mohs relative hardness scale as seen in figure 2.10. This scale is used in the form of a scratch test, if the material being scratched gets a mark on it, than it is softer than the material which is

doing the scratching. Buoy chain steel (1022) has a Mohs relative hardness of about 4-4.5.

Mineral	Mohs relative Hardness	Scratch Test	Rosiwal absolute Hardness	Vickers kp / mm^2
Talc	1	scrapeable with fingernail	0.03	2,4
Gypsum	2	scratcheable with fingern.	1.25	36
Calcite	3	scr. with copper coin	4.5	109
Fluorite	4	easily scr. with knife	5	189
Apatite	5	still scr. with knife	6.5	536
Orthoclase	6	scr. with steel file	37	795
Quartz	7	scratches window glass	120	1,120
Topaz	8	scratches quartz	175	1,427
Corundum	9	scratches topaz	1,000	2,060
Diamond	10	scratches corundum	140,000	10,060

Figure 2.10: Mohs Hardness Scale (Mohs Hardness Scale)

This information is important as chain wear does not often only occur in the interlink region but also occurs on the outside of the chain as it moves across the bottom of the sea bed. The amount of wear that occurs is much dependent on the geographic area that the mooring is placed. This is cited to show this study is not a complete summary of chain wear occurring on a buoy mooring but just a piece of it. In certain scenarios where interlink wear is predominately present, i.e. mud or silty seabed, this study may result in an accurate prediction of chain wear.

2.5 Corrosion

A few studies have been performed in the past that analyzed the use of alternate metals to help slow the effects of corrosive wear on buoy moorings due to abrasion and corrosion. Introduction of high strength steel alloy as chain material can

help extend a mooring chain service life since the harder steel alloy decreases wear and abrasion in service (Paul, Irish, Gobat, & Grosenbaugh, 2007). The results from the tests showed that 4340 steel would yield the best material for buoy chain; this test was confirmed by both laboratory and field experiments.

An empirically based study was conducted in partnership between the U.S. Coast Guard and Canadian Coast Guard to explore the wear rates with these different chain materials. Steel, when immersed in seawater, will experience corrosion through uniform attack, pitting and crevice corrosion. Pitting corrosion was looked at as a major cause of mooring failure when the Canadian Coast Guard performed similar tests with other various alloys (Kohler, 1985). The pitting corrosion appeared to occur on any chain that had less than 0.58 percent Nickel content in it (Danzik, 1986). AISI 4340 was determined to be the best corrosion resistant material. Although it is very corrosion resistant it is also very difficult to manufacture resulting in a high cost to produce. It was determined from a cost-benefit analysis that the 1022 buoy chain the USCG currently uses is the best solution for a buoy chain mooring, although if possible and cost effective Copper-Nickel alloy would be optimal (Danzik, 1986). The present study mainly focuses on the interlink wear where the effects of the sea water corrosive environment are applied but only in the short term. This may help with simulating an accelerated interlink wear but will most likely neglect any pitting corrosion that may occur. Pitting corrosion in 1022 buoy chain was not very apparent in empirical studies, therefore it was concluded that this effect shall not be a main driver of any chain wear occurring while using this type of steel (Danzik, 1986).

CHAPTER 3

METHODOLOGY

The movement of a floating body in a random seaway comes from both wave theory and empirical testing; more often than not the prediction is not an exact replica of what will occur in the real environment but a close prediction can be made. Regardless of how the floating body moves, if it is secured to the bottom through use of a catenary chain system, wear is going to occur which is a function of tension, sliding distance, material attributes and a wear constant. The wear constant is what the experiments of this study will yield; this will be applied to the Archard formula to output total chain wear.

Buoy motions were computed by inputting the equations and wave spectrum defined in section 2.3 into MATLAB. Inputs for the current and wave data along with buoy geometry are defined to help vary the problem so that it may apply to most environments seen in the area of responsibility for the Coast Guard. The buoy geometry is assumed to be a perfect cylinder, although most buoys do not have this shape it is a solid starting point since there have been many studies performed on floating cylinders in a seaway.

3.1 Wear Experiments

In order to determine the wear rate coefficient (K from equation 2.28) an experiment was conducted by cycling a chain in a vertical sinusoidal motion under its own weight and measuring chain wear over a period of time. The controlled variables

for this experiment are noted in table 3.1. Frequency has a maximum value of 2.5 Hz and height has a maximum value of approximately 7.25 inches due to equipment limitations. The amplitude of chain motion for the first and second set of experiments was set at 6.5 inches and 7 inches, respectively. This distance was determined by finding the maximum height at which the chain could rotate without lifting the sinker off the bottom of the tank.

Symbol	Parameter Description	Units	Type
F_n	Normal Force	ML/T^2	Variable
S	Sliding Distance	L	Controlled Variable
F_f	Frictional Force	ML/T^2	Variable
f	frequency of load	1/T	Controlled Variable
h	amplitude of motion	L	Controlled Variable
W	Wear Volume	W	Variable
‰	Salinity	M/L^3	Controlled Variable

Table 3.1: Analytical and Experimental Parameters

Experiments were completed with two different types of water, varying salinity (artificial seawater and distilled water) while varying the amount of time the chain cycled in each solution. The artificial seawater is prepared in accordance with ASTM D 1141-52 Formula a, Table 1, section 4 (156 grams of salt compound per gallon of distilled water). The time the experiment was run ultimately varied the sliding distance which yielded the wear volume.

Test	Water Type	Cycle Time (hours)
1	Distilled	1
2	Distilled	2 (test 1 + 1 hour)
3	Distilled	3 (test 2 + 1 hour)
4	Distilled	4 (test 3 + 1 hour)
5	Distilled	5 (test 4 + 1 hour)
6	Artificial Seawater	1
7	Artificial Seawater	2 (test 1 + 1 hour)
8	Artificial Seawater	3 (test 2 + 1 hour)
9	Artificial Seawater	4 (test 3 + 1 hour)
10	Artificial Seawater	5 (test 4 + 1 hour)

Table 3.2: First set of experiments varying solutions and cycle time

Test	Water Type	Cycle Time (hours)
1	Artificial Seawater	Approximately 6 hours
2	Artificial Seawater	Approximately 6 hours
3	Artificial Seawater	Approximately 6 hours
4	Artificial Seawater	Approximately 6 hours

Table 3.3: Second set of experiments varying cycle time

The experiment was performed as follows:

1. Chain used was ½ inch 1022 low carbon steel buoy chain available at the local Aids to Navigation Team in Bristol, Rhode Island. This chain has welded links and is of the same scaling as the remainder of USCG buoy chain as per USCG Specification 121032 Rev H (appendix A.2).
2. The simulated wave height was determined by adjusting arm length on electric motor.
    a. For the first set of experiments, the frequency of the motor was set at 150 RPM (2.5 Hz) but was slowed to about 138 RPM with use of

a variable autotransformer also known as a Variac (see figure 3.1). A rotational speed of 138 RPM was determined as it was the slowest the original motor could spin the chain without stalling.

Figure 3.1: Variac used to slow speed of motor in the first experiment.

b. The second set of experiments was completed with a slower motor and use of a motor drive; this helped get the rotational speed low enough (approximately 61 RPM) so the accelerations of the chain were small enough that it would stay in contact with all surfaces the entire time.

3. Chain was connected to motor via a system of aluminum plate connections and directed perfectly in the vertical direction via a stainless guide rod and slide (see figure 3.2).
4.
    a. First set of experiments: the motor was run for specific intervals of one hour in both fresh (distilled) and salt water.
    b. Second set of experiments: the intervals were much longer (approximately 6 hours) and the chain was only oscillated in the artificial sea water. Total cycle count was used when calculating total chain movement.
5. Dry mass of entire chain length was measured after each time interval. The wear diameter of a specific link was to be determined.
6. In the first set of experiments only, another chain was cut to the exact same length as the experimental chain and used as the control chain to determine corrosion affects in still water. This chain was placed in the specific fluid without any movement, after each experiment it was dried and weighed.

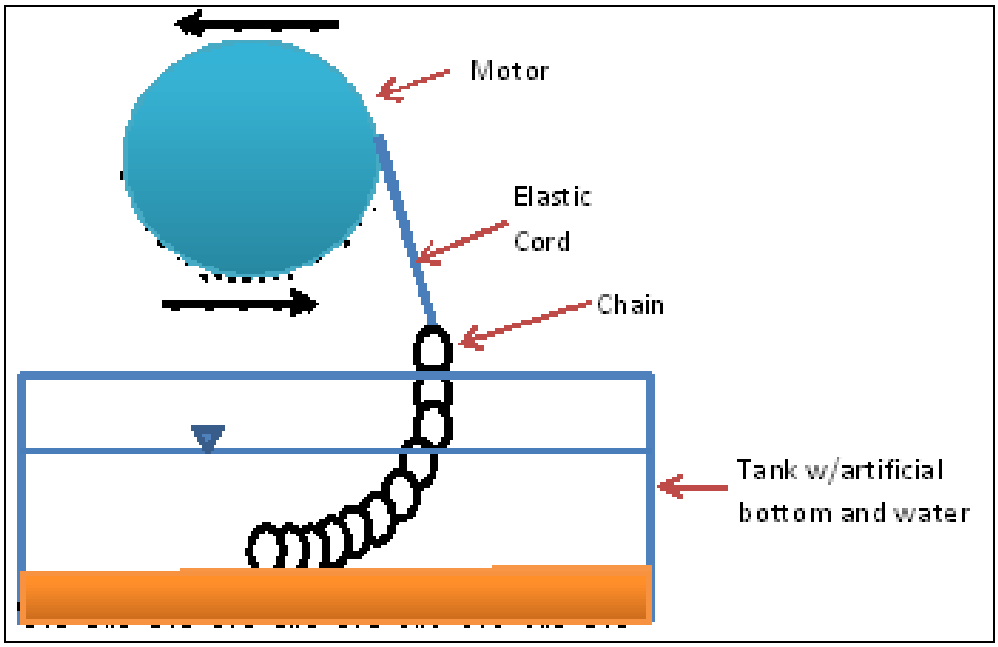

Figure 3.1a: Proposed experimental set up

Figure 3.2: First experiment, chain attached to motor via slide apparatus.

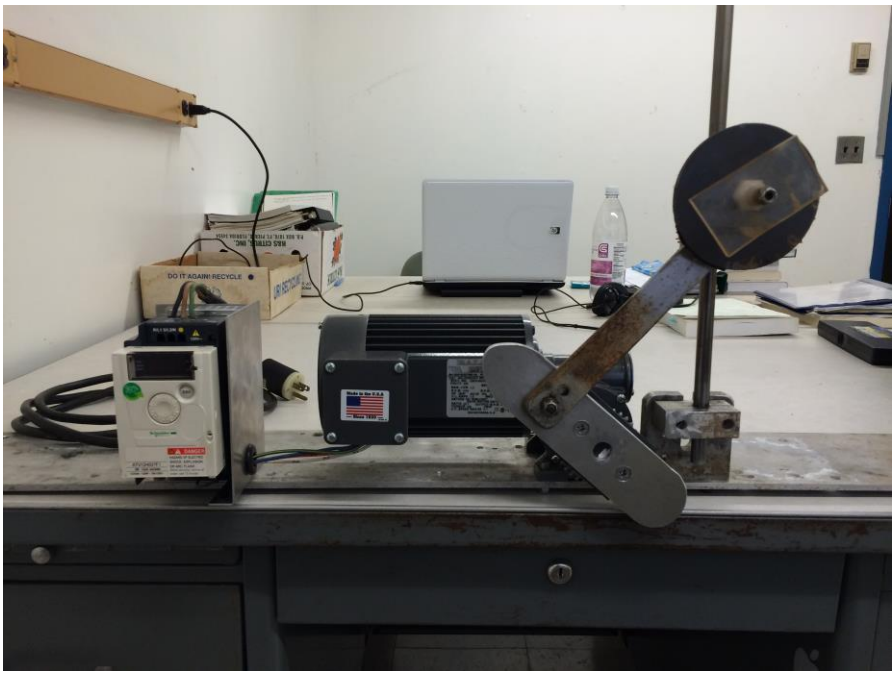

Figure 3.3: Second experiment, new motor and slide apparatus.

Three sets of pi groups were determined using variables from energy potential parameters. These pi groups are show in tables 3.4 to 3.6.

Symbol	Parameter Description	Units	Type
μ	Potential	ML^2/AT^2	Variable
U	Energy	L^2M/T^2	Fixed
P	Pressure	M/T^2L	Variable
V	Volume	L^3	Variable
T	Temperature	t	Variable
S	Entropy	L^2Mt/T	Fixed

Table 3.4: Variables for pi group I

The variables for pi group 1 were based on the internal energy-pressure (equation 3.2) and the internal energy of an elastic solid. Variables for force-modulus contact and

surface energy-diameter (pi groups II and III, respectively) were determined by using equation 3.1 and determine which physical characteristics of the system are known as well as which ones are to be determined.

$$\Delta U = Q - W = TS - PV \qquad (3.2)$$

Where Q is heat transferred into the system, W is work done on the system.

Symbol	Parameter Description	Units	Type
F_n	Normal Force	ML/T^2	Variable
E	Modulus of Elasticity	M/T^2L	Fixed
a	Radius of Contact	L	Variable
d	Diameter of Chain	L	Variable

Table 3.5: Variables for pi group II

Symbol	Parameter Description	Units	Type
R	Roughness	L	Variable
E	Modulus of Elasticity	M/T^2L	Fixed
γ	Surface Energy	M/T^2	Fixed
F_n	Normal Force	ML/T^2	Variable
d	Diameter of Chain	L	Variable

Table 3.6: Variables for pi group III

The following π groups were yielded from Buckingham Pi Analysis via tables 3.4 to 3.6:

$$\pi_1 = \frac{FV}{Ua} \quad \text{(Internal Energy-Pressure Parameter)} \qquad (3.3)$$

$$\pi_2 = \frac{F}{Ed^2} = \frac{F}{Ead} = \frac{F}{Ea^2} \quad \text{(Force-Modulus Contact Parameter)} \qquad (3.4)$$

$$\pi_3 = \frac{ER}{\gamma} = \frac{F}{\gamma d}$$ (Surface Energy-Diameter Parameter) (3.5)

The π groups (equations 3.3 to 3.5) were used to help plot the results of the experimental data. Since this data is non-dimensionalized, best fit regressions can be determined from the results and with known variables from a scaled up system it can provide empirical outputs that will help determine characteristics about the wear throughout the chain. These correlations are a critical part of this study since they will pinpoint the weakest links in the chain as well as what vehicle may be causing the link to wear excessively. These empirically derived results along with the on-site chain wear often recorded by AtoN units in the form of Annual Chain Wear (ACR) recorded in the USCG's IATONIS program were used to help validate the program's ability to predict chain wear as seen in appendix A.6.

3.2 Wear Algorithm

To determine the wear within a chain, an algorithm was created as a step-by-step guide mapping a course to determine the link with the most wear as well as the remaining chain strength. This algorithm in its most basic form is shown in figure 3.4 and is the building block for the MATLAB code that will be generated. This MATLAB program will use the algorithm in figure 3.4, performing both frequency and time based calculations to determine the point at which most chain wear occurs through multiple iterations.

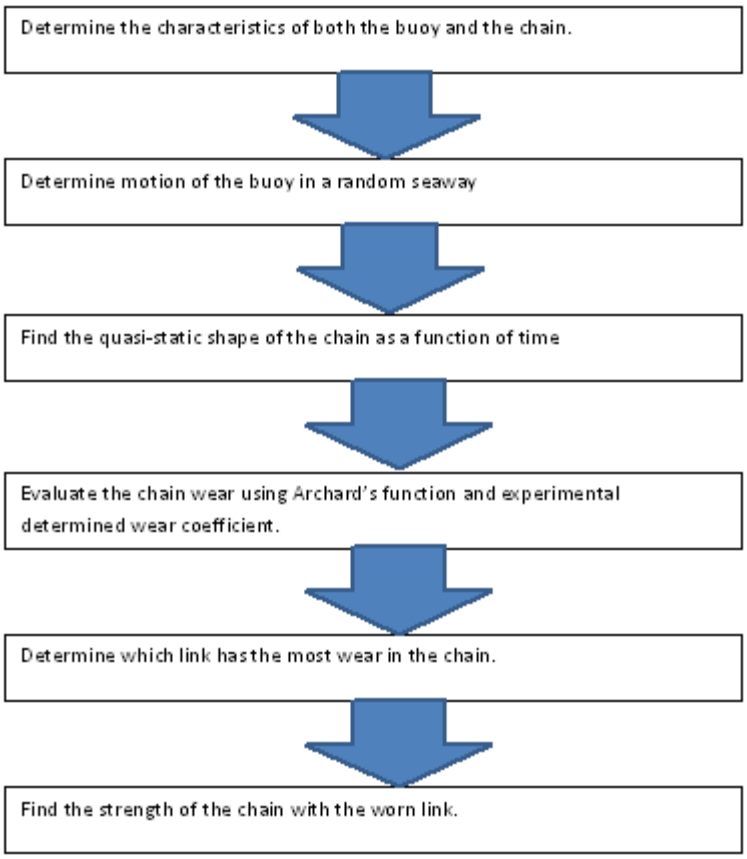

Figure 3.4: Algorithm for determining chain wear.

CHAPTER 4

RESULTS

This chapter presents and discusses all of the data collected during the laboratory testing. Testing was performed using the equipment and methods specified in the previous chapter.

The oscillation testing performed yielded three measured characteristics; mass, roughness and link diameter. Analyzing the data from all three indicated that they all reduced at some rate due to the wear caused by the motion of the chain. The results were then plotted in the form of non-dimensional parameters to provide regressions that could be used to predict chain wear values in a full scale environment as well as implementation into the MATLAB based wear program.

4.1 Experiment I

If chain wear was to be measured utilizing a real life experiment, the experiment would be required to run for extended periods of time; the purpose of these experiments was to speed up the cycling of the chain to help yield similar experimental results without having to wait as long. In experiment I the chain was cycled at a rate of 138 revolutions per minute which was the slowest the motor could be turned with the load of the chain without stalling. Although this may seem slow, it was very quick for the chain resulting in more than two cycles per second; the chain accelerated faster than the speed of gravity causing the contact points to separate

during the down stroke of the motor. The results of the first experiment (experiment I) were implemented into each of the determined parameters from chapter 3 to help plot trends to validate data and use regressions for full scale implementation. Looking more closely at the parameters, it is observed that the regression from Force-Modulus Contact (figure 4.2), a function of cycles, tension, diameter, contact radius and modulus of elasticity, can be solved for the contact radius if tension, chain diameter and number of cycles are known; each easily determined analytically.

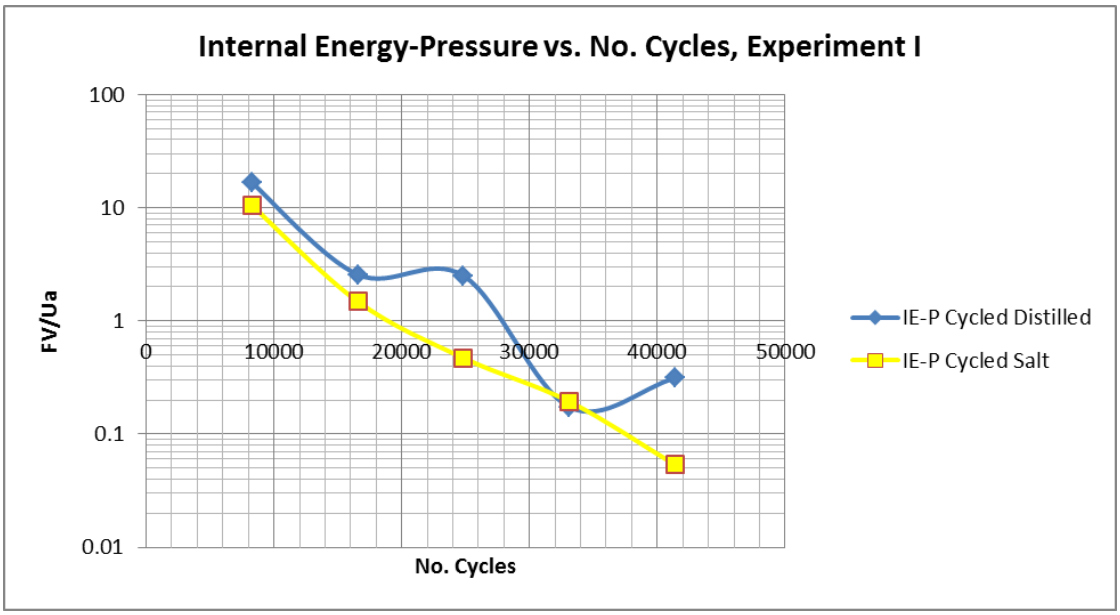

Figure 4.1: Internal Energy-Pressure vs. No. Cycles

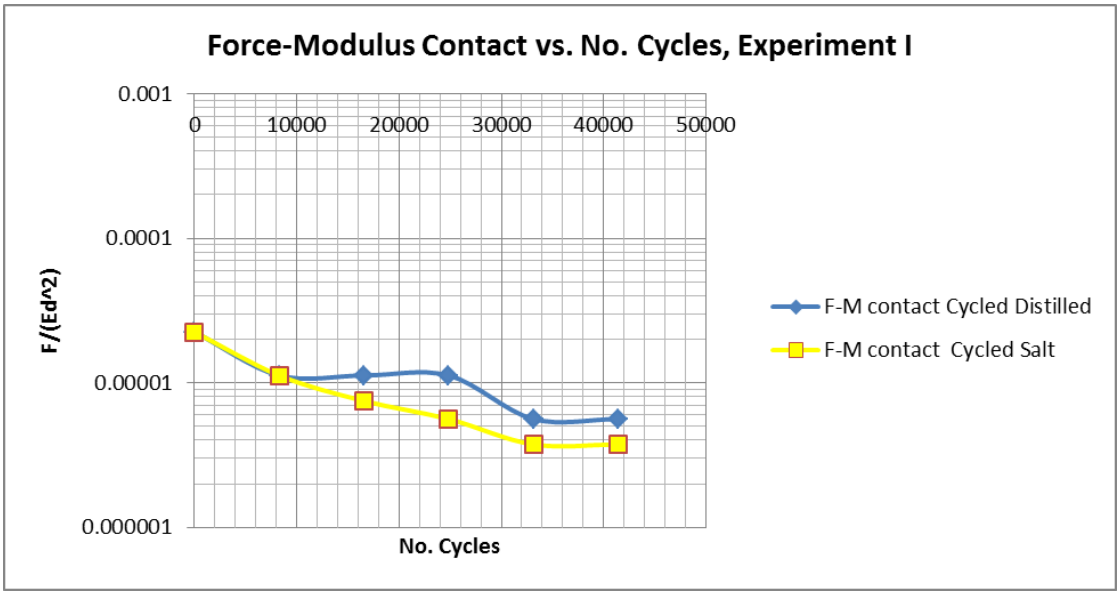

Figure 4.2: Force-Modulus Contact vs. No. Cycles

Once the contact radius is obtained, Internal Energy-Pressure (IE-P) can then be solved for wear volume. IE-P is a function of wear volume, contact pressure, energy and cycles. The energy value used for IE-P was the surface energy for iron oxide; this was used since the chain is always corroding, therefore there will be some level of iron oxide forming (however small it may be) on the surface of the chain between cycles. As noted in figure 4.1, the value of IE-P in experiment I for the chain immersed in distilled water was slightly higher than the chain immersed in artificial salt water. The regression does not fit very well on the distilled chain IE-P date; more experimental testing would need to be completed to further validate these results.

For the Surface Energy-Diameter (SE-D) parameter used in experiment I, it is a function of diameter, surface energy, tension and cycles. The diameter of the chain as it became worn was the variable in question as it is plotted across the number of

cycles the chain moved. The wearing surfaces were measured by way of six inch calipers, Cen-Tech Model 92437, see figure 4.3.

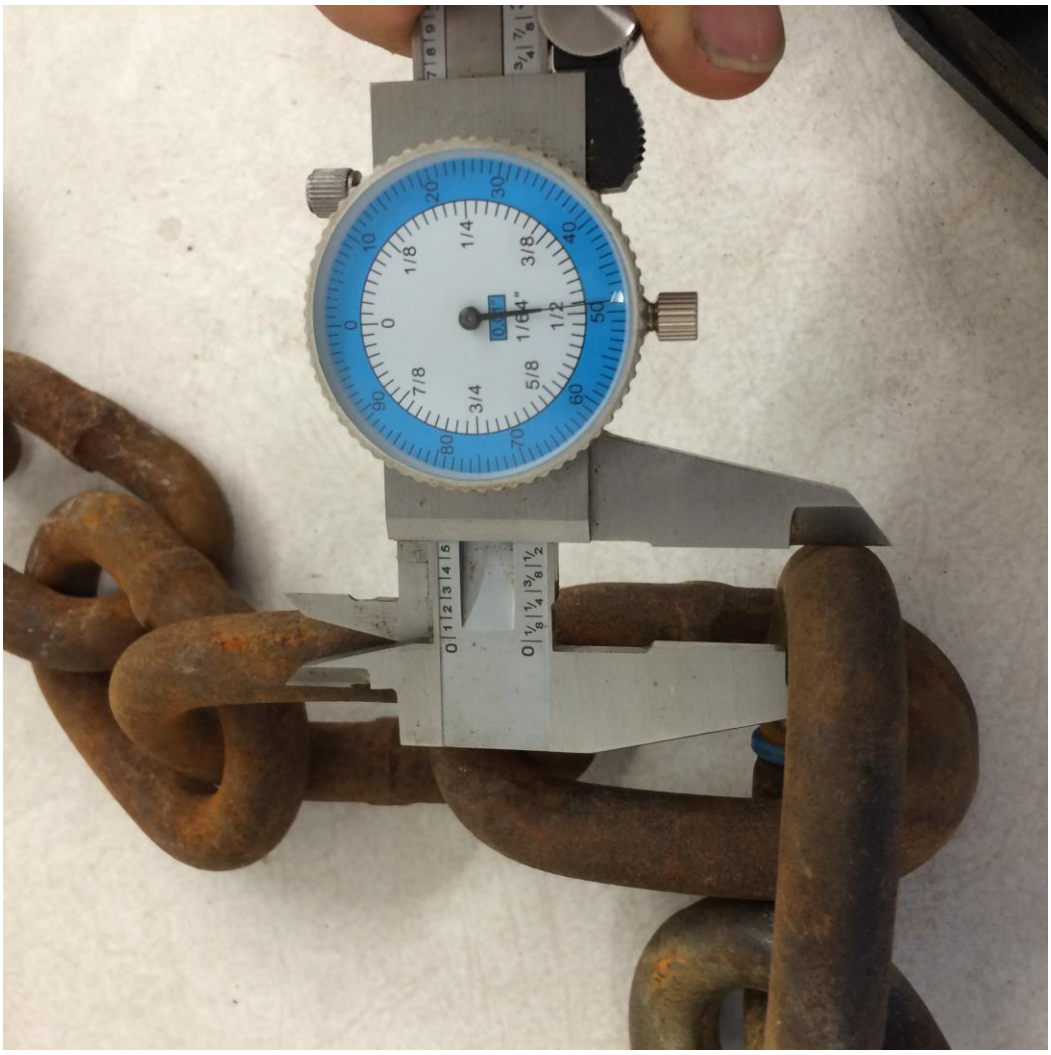

Figure 4.3: Measuring chain wearing surface with calipers

With a regression formed from this parameter, the diameter of a chain can be determined over time if the material properties and tension in the chain are known.

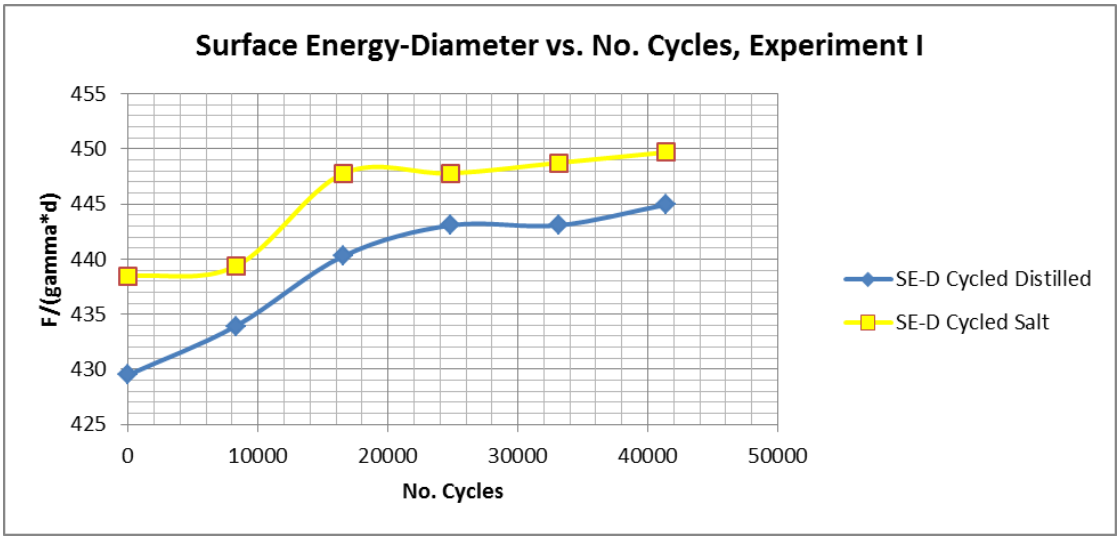

Figure 4.4: Surface Energy vs. No. Cycles

The SE-D parameter does not provide much information in experiment I since there would need to be much more experimental testing completed to allow for appreciable wear of the link diameter allowing for an accurate regression to be mapped. Another option would be to measure surface roughness and implement into the SE-D parameter, a method that was employed for the second round of experiments.

Using the data collected, the wear coefficient was calculated using a different form of the Archard equation solving for K as seen in equation 4.1. The 'F' term or tension was determined through analysis of the chain weight and acceleration. Two values for the tension of the chain at the peak and trough were both determined and averaged together to get average tension through the links that were rotating.

$$K = \frac{WH}{Fs} \tag{4.1}$$

Where:

W is the wear volume.

H is the material hardness measured in units of force per area

s is the total sliding distance of the material

F is the force normal to the wear or tension

The sliding distance was assumed to be the arc length of 90 degrees for each link diameter. Some link-to-link surfaces rotated 90 degrees; some did twice as both links rotated from the horizontal position to the vertical position. With the sliding distance assumed, the total wear volume was calculated by taking the density of chain and multiplying it by the change in mass between experiments as seen in figure 4.5. The mass was measured using a Denver Instrument Company scale, Model XL-3K, serial 60994 and was calibrated by the Central Scale Company on August 3, 2013 certified for approximately one year, see figure 4.6.

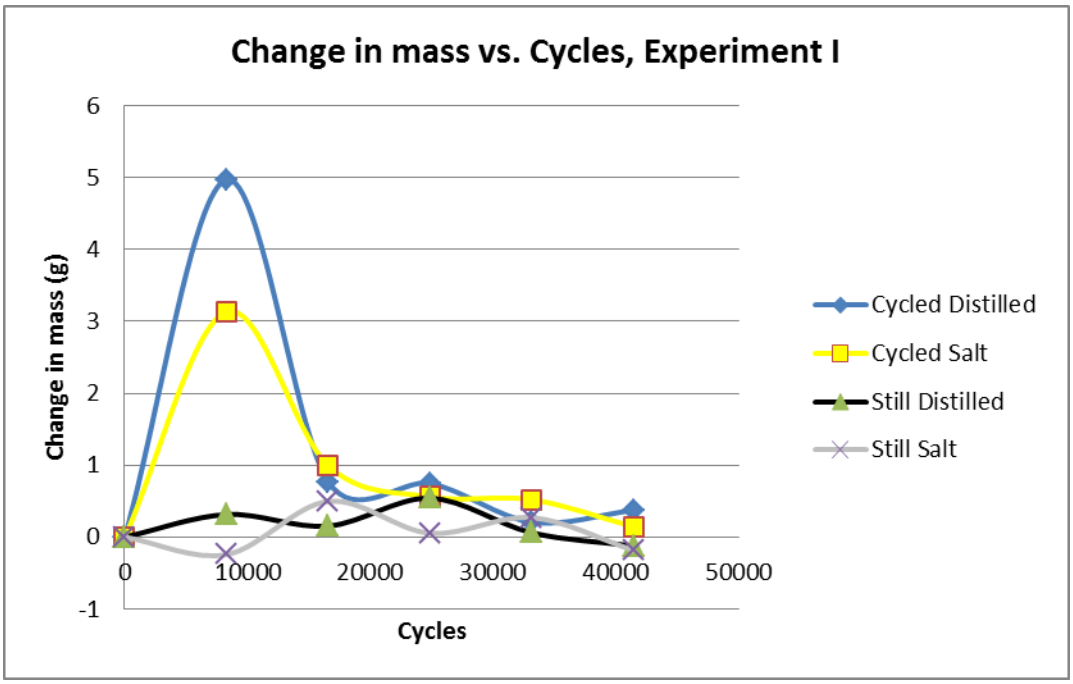

Figure 4.5: Mass of chain vs. cycles.

Figure 4.6: Scale used to measure mass of chain.

Material hardness is assumed to be a constant, with all the parameters known, the wear coefficients for both the distilled and salt chains were determined as seen in figure 4.7. The peaks seen in figure 4.7 during the first 10,000 cycles were most likely a result of wear in of the chain as well as the sheading of iron oxide formation.

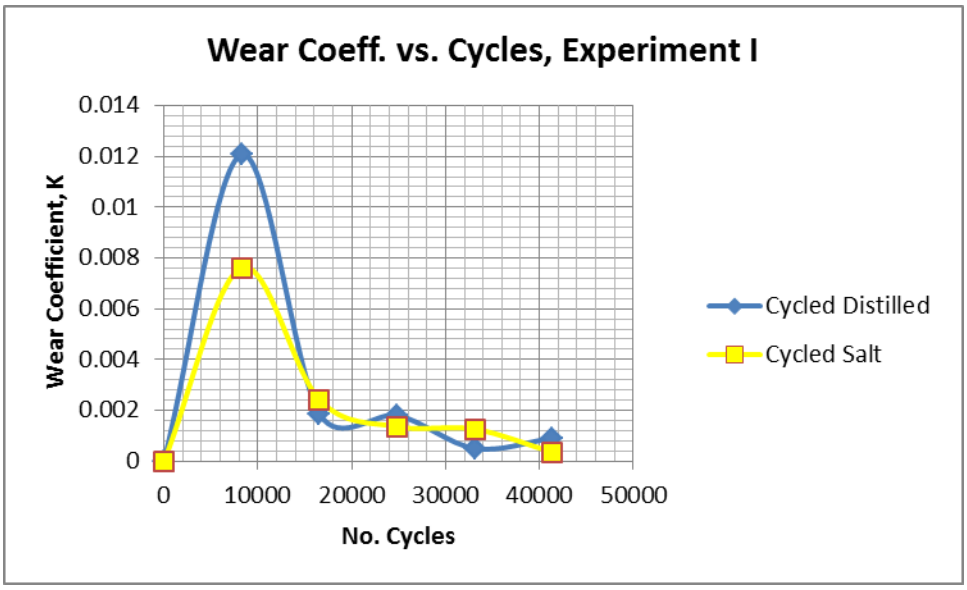

Figure 4.7: Wear coefficient vs. Cycles

The wear rate coefficient rapidly decreases and then the slope for both distilled and salt solution chains is approximately the same. Due to the many assumptions and chain hoping, this data was not used and a second experiment was conducted as seen in table 4.1a. The chain's inertia would cause it to fly out of the water due to the high rate of speed at which would cause the chain contact not to be consistent. Since the contact is not consistent, this will invalidate the sliding distance assumption made as well as further stretch the assumption of an average normal force between the chain links. It will be shown later that these calculations of the wear constant K in the first

experiment are actually low resulting in a low prediction of wear occurring in the chain.

		Dimensionless Constant K	
Time (hours)		Cycled Distilled	Cycled Salt
0	0	0	0
1	8280	0.012075083	0.007612729
2	16560	0.001862689	0.002413397
3	24840	0.001814097	0.001360573
4	33120	0.000502116	0.001263389
5	41400	0.000907049	0.000348242
6	49680	0	0
7	57960	0	0
8	66240	0	4.46286E-05
	Average	**0.003432207**	**0.002173826**

Table 4.1: Wear constant K determination in both distilled and salt water.

Chain diameter was also measured during this experiment as seen in figure 4.8. The link diameter did not have any change with the control chain sitting in distilled water but the chain immersed in salt water did have an initial increase in link diameter that could be excess iron oxide formation. The cycled chains did have some slight chain wear, which was to be expected. Unfortunately, the chain was not cycled enough to get any appreciable chain wear that would yield a regression that could be applied to a full scale system.

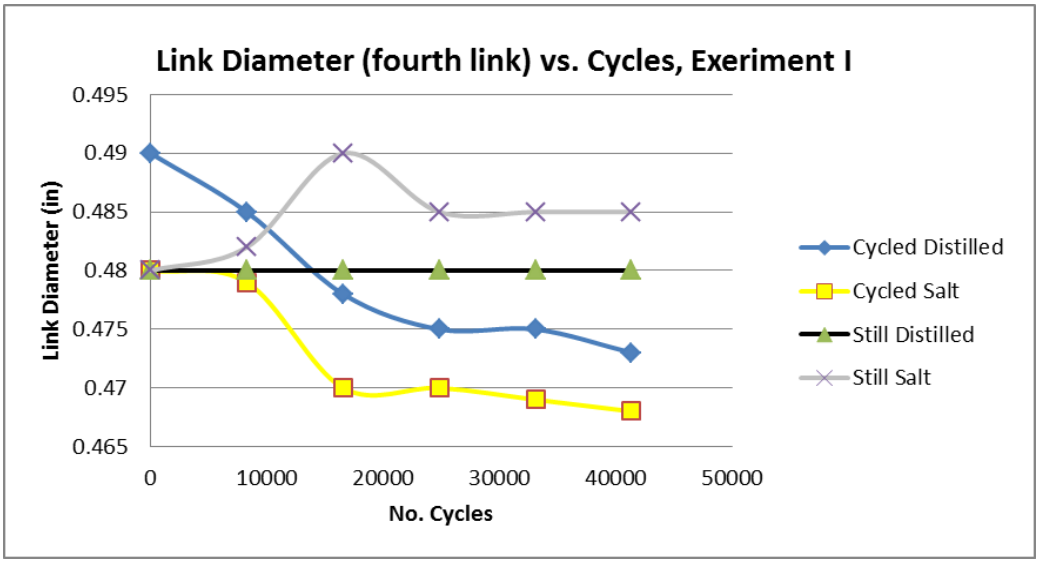

Figure 4.8: Link diameter versus cycles, first experiment.

4.2 Experiment II

After the first round of experiments, the machinery used was deemed to have excessive speed resulting in the chain accelerating faster that the acceleration of gravity due to the machine rotating at 138 revolutions per minute which caused the wearing surfaces to lift off and collide, possibly causing inaccurate data. The speed at which that equipment moved was the slowest it could run before the motor stalled, therefore new equipment needed to be utilized.

A new motor and drive were procured allowing the motor to spin at rotations from 83 revolutions per minute all the way down to a stopping speed providing a large range of speed control for this experiment. The purpose of these experiments was to still provide an accelerated chain wear simulation while also keeping the chain links touching at all times. This is a key point since the wear rate is measured through a few parameters, one of them sliding distance, if the chain links are not in contact with one another the sliding distance calculation will be inaccurate. The fastest speed at which

the motor was run without allowing the chain links to separate was 61 revolutions per minute, or approximately one hertz.

Another change that was made to the second round of experiments was the measurement of surface roughness within the interlink surface. The surface roughness was determined using a Mahr, MarSurf XR 20 Perthometer.

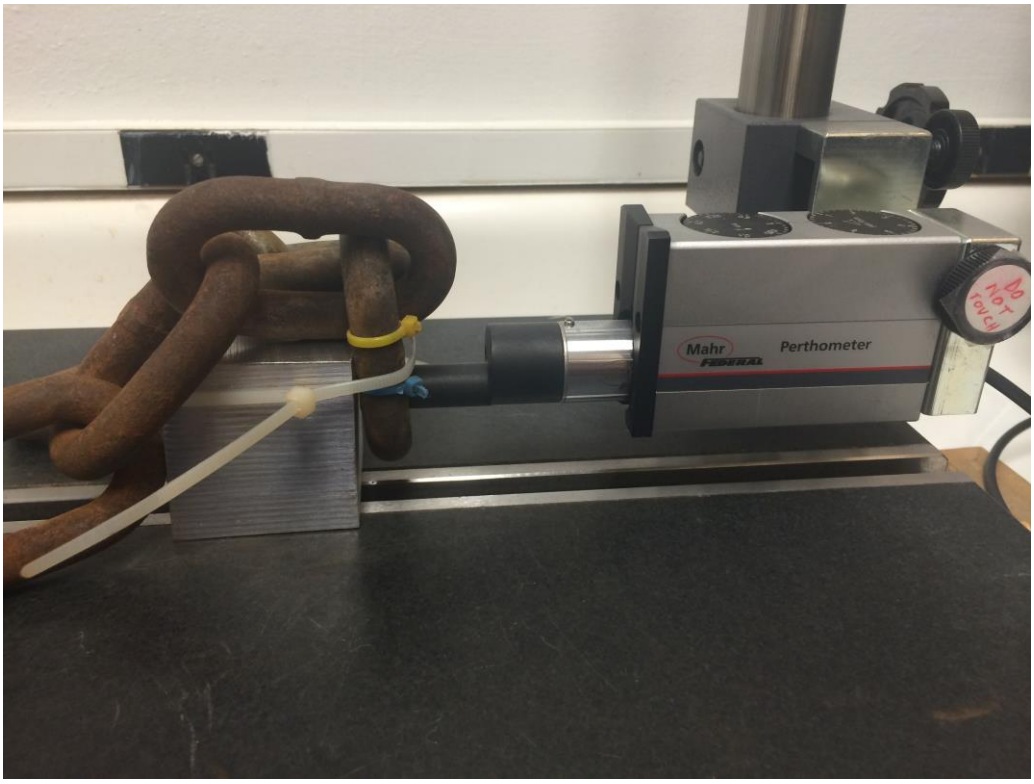

Figure 4.8a: Surface roughness measuring tool, Mahr MarSurf XR 20.

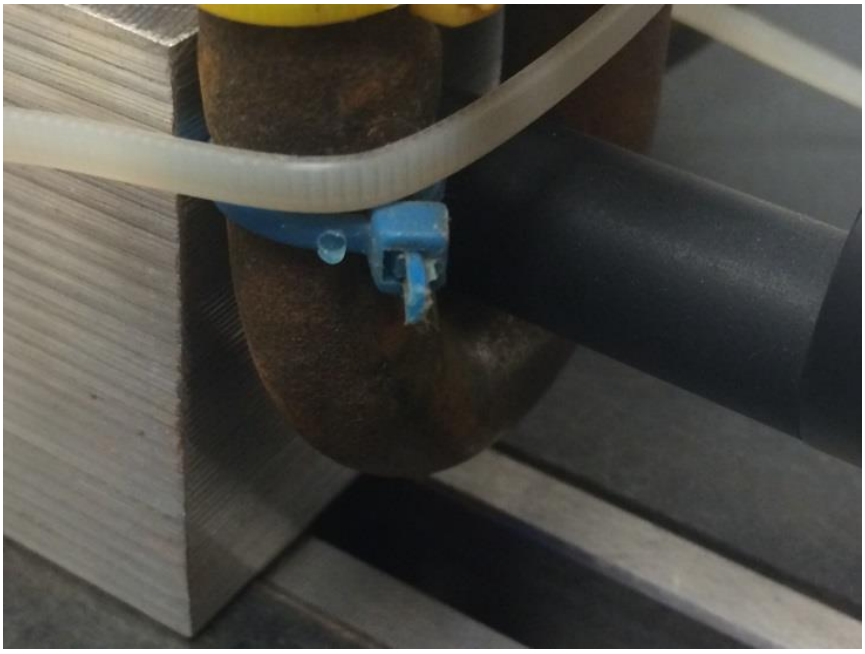

Figure 4.8b: Roughness measurement (Note: orientation of yellow and blue zip ties consistent through each experiment to ensure correct wear surface is measured)

The roughness parameter would be used in the SE-D calculation and can empirically determine how surface roughness will change when the links slide against each other over a set amount of cycles (see figure 4.8d). The empirically derived value of surface roughness can be used when analytically determining the change in energy potential in equation 3.1.

Figure 4.8c: Wear Surfaces. (left) surface at end of second round, (right) surface at end of fourth round.

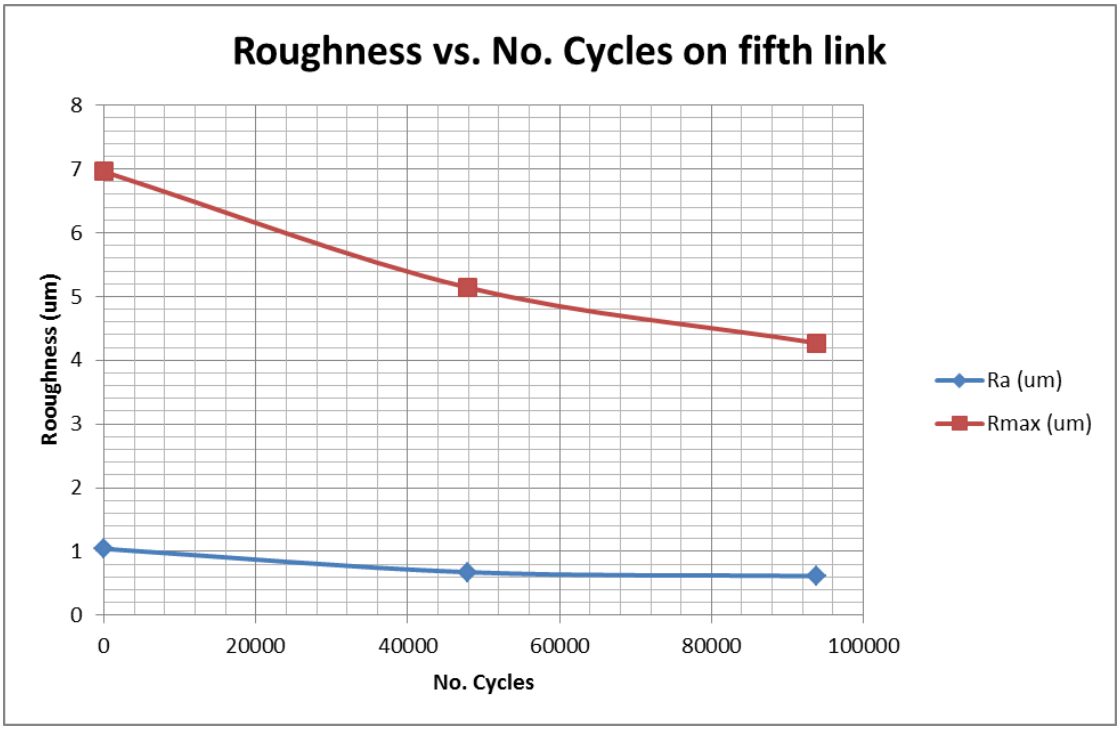

Figure 4.8d: Roughness versus Cycles for experiment two.

The F-MC calculation will be used again to empirically predict changes in the contact radius over cycles (figure 4.10) which will then be used to determine the contact pressure, the independent variable in IE-P. When IE-P (figure 4.9) is known, the wear volume for the system will be determined. Again, this is based on the constant for surface energy of iron oxide as the 'U' term.

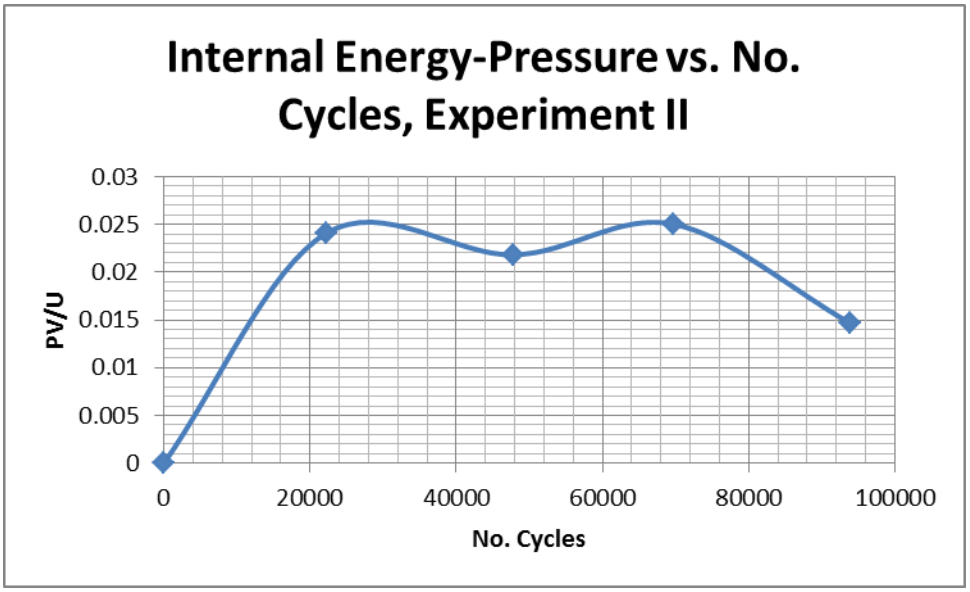

Figure 4.9: Internal Energy-Pressure vs. No. Cycles

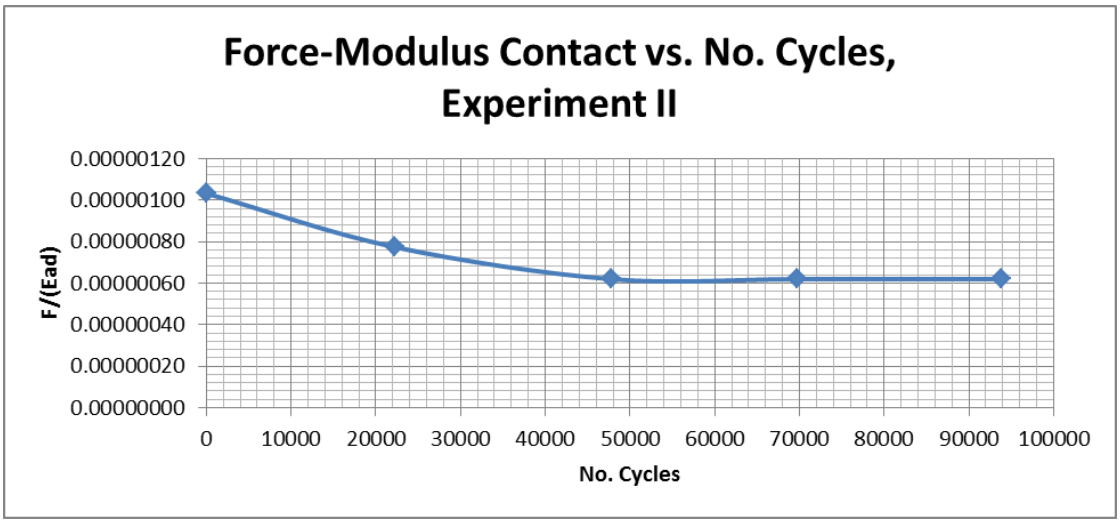

Figure 4.10: Force-Modulus Contact vs No. Cycles

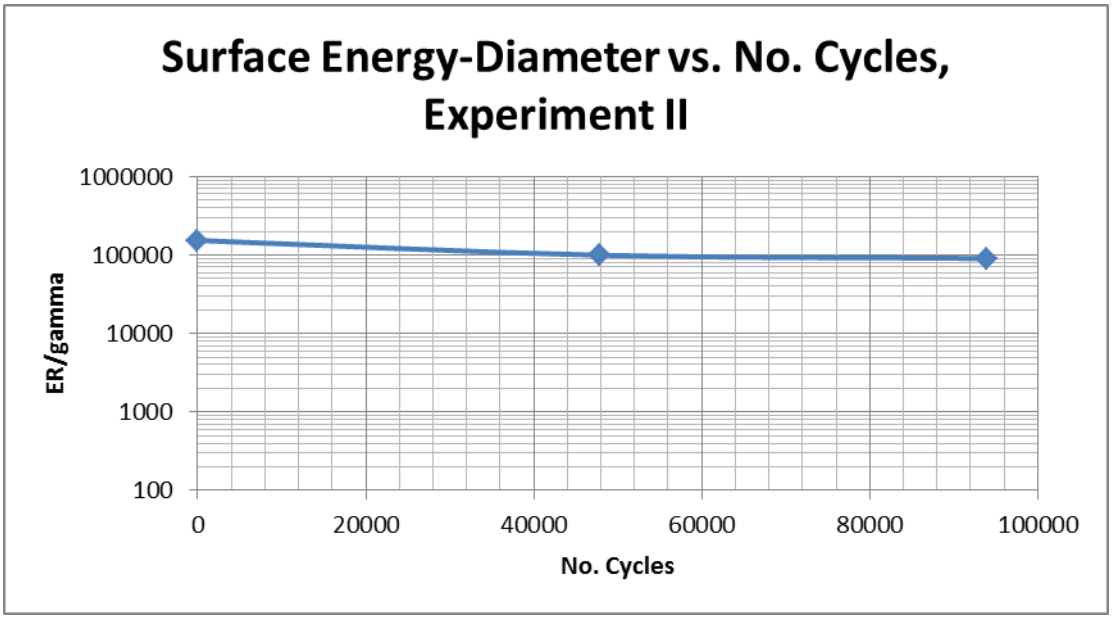

Figure 4.11: Surface Energy-Diameter vs. No. Cycles

A linear regression for the data in graphs of IE-P and F-MC was attempted, but the 'R squared' value or a regressions ability to plot over the majority of the data was low for both; extensive experimental testing would need to be completed to validate these results and assign regressions, if any. The results for SE-D seem fairly accurate, yet again the linear regression did not yield an accurate depiction of the results; therefore an exponential equation was used as noted in figure 4.11.

During the first experiment as mentioned earlier, tension in the chain was determined by calculating the rate at which the chain oscillated then analytically determining the tension in the chain at the point of interest. In the second experiment, a scale (Accu-Weigh by Yamato Model T-10) was used to measure the actual tension in the chain as seen in figure 4.12. The tensions at the peak and trough points of the movement were statically measured and corrected by adding the weight of each link below the point of measurement to the contact of interest. Both values were averaged

to yield an average value of 2.00 newtons of force (table 4.1). This was significantly less than the first experiment, most likely due to conservative estimates and analysis of the fourth link tractions whereas the second experiment analyzed the fifth link tractions. If a more accurate measurement was desired, a load cell would need to be placed within the chain and attached to a computer so that the tension could be recorded throughout the cycle taking into account the effects of added mass and interlink friction during dynamic motion.

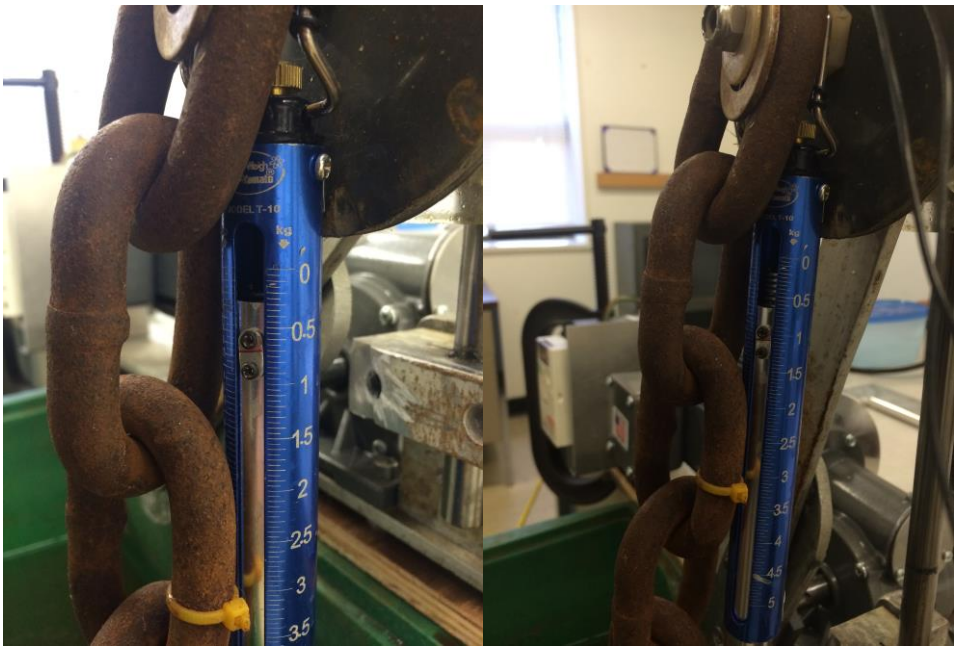

Figure 4.12: Determining tension within chain. Right: up stroke, Left: down stroke.

With the tension in the chain determined, it was necessary to determine the sliding distance. As mentioned in seciton 4.1, the first experiment assumed that the links with traction had full 90 degree rotation which resulted in higher sliding distances that may have contributed to possible innacurate wear coefficinets. During the second experiment, the chain was moved through its cycle and an approximate

value of each chain rotation angle was determined by directly measuring the angle over which wear occured.

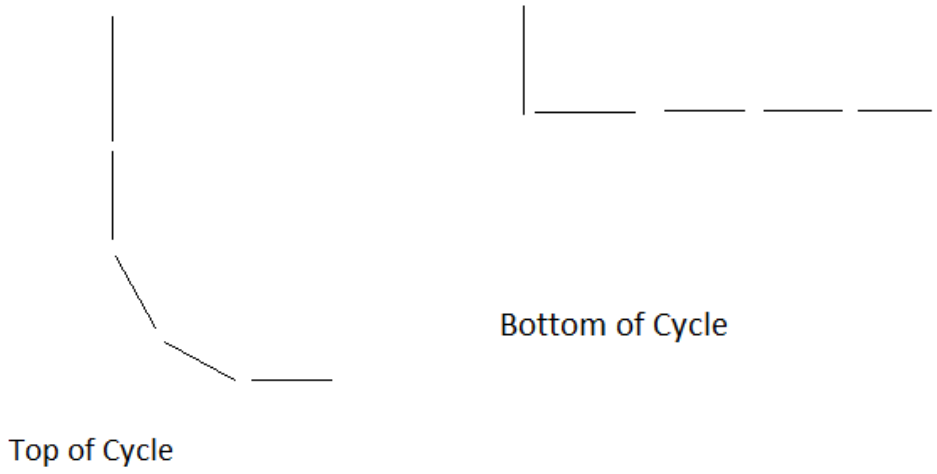

Figure 4.12a: Shapes of the experimental chain at the top and bottom of each cycle.

Location	Fn up (N)	Fn dn (N)	Avg Fn (N)	SD/cycle (m)	Rot. @ wear sfc (deg)
Wear link	5.93	2.00	3.97	0.0199	90
1 link below WL	4.31	0.00	2.15	0.0133	60
2 links below WL	2.69	0.00	1.34	0.0100	45
3 links below WL	1.06	0	0.53	0.0066	30
Total			**2.00**	**0.0499**	

Table 4.2: Tension and sliding distance

The total sliding distance was approximately 0.05 meters per cycle of the chain. Wear mass change (figure 4.13) was determined the same as it was in the first experiment and the material hardness value also remained the same. With these values, the wear coefficient, K in figure 4.14 was determined. The wear coefficient appeared to fit very well to an exponential regression with a high R-squared value as per figure 4.14. For

the MATLAB program, the K coefficient used was the average of the K values, resulting in a value of 5.2 x 10^{-3} as seen in table 4.2a.

Experiment	Time (minutes)	Cycles (total)	Dimensionless Constant K
0	0	0.0001	0
1	364	22204	0.00438476
2	420	47824	0.005380977
3	360	69784	0.00719997
4	395	93879	0.003846689
		Average	**0.005203099**

Table 4.2a: Average value of the dimensionless wear constant, K.

Comparing the average value to those of Archard, the results were considerably close to the K coefficient for mild steel on mild steel of 7 x 10^{-3} (Gutierrez-Miravete). This curve has a much better fit than any curve that could be fit to the wear coefficient results in the first experiment.

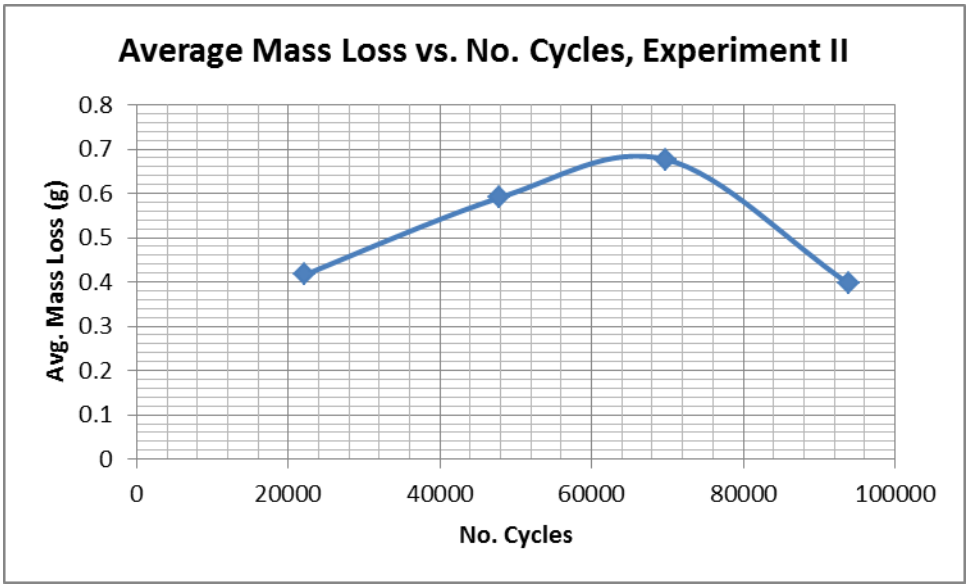

Figure 4.13: Average mass loss in chain versus cycles.

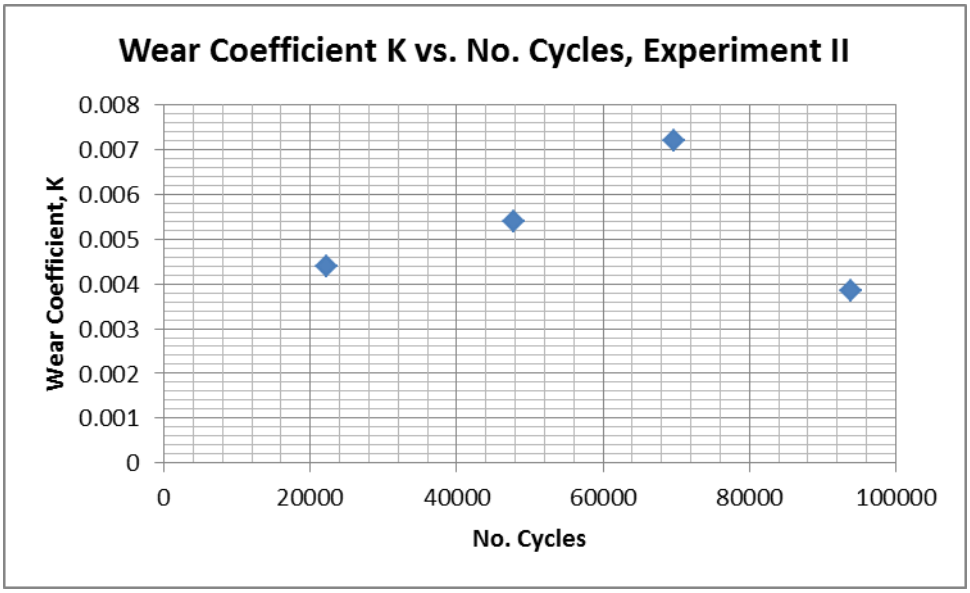

Figure 4.14: Wear coefficient versus cycles.

The diameter of the chain at the point of interest (fifth link from the bottom), was also analyzed to determine if there was any appreciable wear between the links during this short test. From the results, it appears the link diameter did not change much as seen in figure 4.8. It would be difficult to map out the wear as a function of chain link diameter size with such a short test. Since steel in general is a fairly good wearing surface, the tests would have to be run for an extended period of time in a controlled environment to yield significant results.

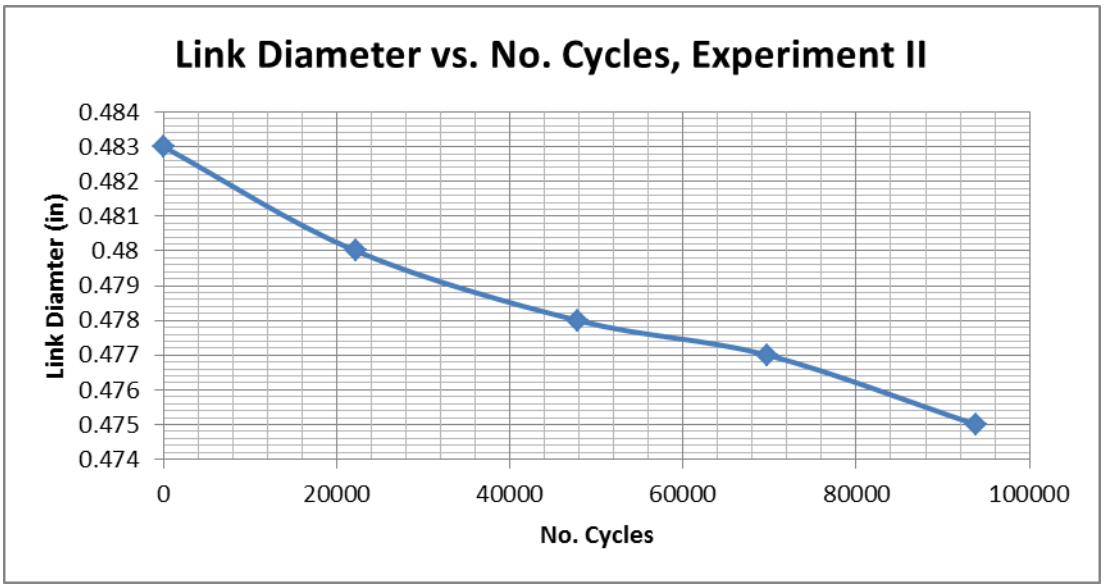

Figure 4.15: Link diameter versus cycles.

4.3 MATLAB Results

Using the MATLAB program to predict chain wear was somewhat successful. The program, when implemented using data from appendix A.6 provided by USCGC FRANK DREW yielded results that were close to the Annual Chain Wear (ACW) measurements. The data used for the wave spectra was from Wave Information Systems (WIS) station 63197. Value for average wave height was averaged over a 20 year period from 1980 to 1999. This data was then converted into significant wave height by multiplying by a factor of 1.6 for a Rayleigh Distribution (Goda, 2010). The significant wave height placed into MATLAB for this information was 1.42 meters. Significant wave period was used by implementing the significant wave height into the correction formula provided by Goda as seen in equation 4.5 (Goda, 2010).

$$T_{1/3} \cong 3.3(H_{1/3})^{0.63} \tag{4.5}$$

The buoys listed in appendix A.6 are 8x26 LR buoys that are approximately 8 feet in diameter and displaced approximately 12,000 pounds (noted in appendix A.5). ACW measurements from A.6 were subtracted from the original chain diameter of 1.5 inches to get the '1 year Actual Chain Diameter' in inches and compared to the output from MATLAB in table 4.3. It can be noted that the MATLAB calculations are within 3 percent of the actual chain wear. These results were compared with those of equation 2.1 and found to be much more accurate (table 4.3). Since these chains are all worn about the same as seen in table 4.3, the maximum yield and tensile forces the chain would be capable of withstanding when worn would be approximately 48,500 and 87,600 pounds, respectively. This calculation assumes a yield and tensile strength of 1022 steel of 34,100 and 61,600 pounds, respectively.

Buoy	Bottom Type	1 year Actual Chain Dia (in)	1 year MATLAB Chain Dia (in)	Percent Error (%)	1 year MSG Chain Dia(in)	Percent Error (%)
Chesapeake Bay LB 12	Sand	1.28125	1.3169	2.78	0.1379	89.24
Chesapeake Ch LB 4	Mud	1.34375	1.3146	2.17	0.1379	89.74
Thimble Shoal Ch LBB 1TS	Mud	1.35625	1.3163	2.95	0.1379	89.83

Table 4.3: Results of running MATLAB program for a one year simulation.

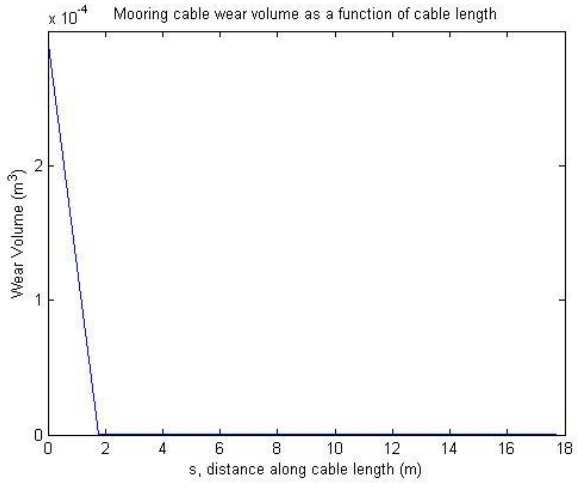

Figure 4.16: Final wear volume over length of chain after running simulation.

The MATLAB algorithm goes through the flow chart as shown in figure 3.4 and is split up into three different sub programs, the RAO for the buoy as a function of frequency, the motion of the buoy as a function of time and the wear calculation. Each of these sub programs utilize equations called out in chapter 2 as well as geometries specified in the appendices. Sample outputs are shown in figures 4.17 through figures 4.25. The RAO calculations are for the 8x26 LR buoy (Chesapeake Bay LB 12 from A.6) in the JONSWAP sea spectrum specified by a significant wave height of 1.42 meters and period of 4.11 seconds.

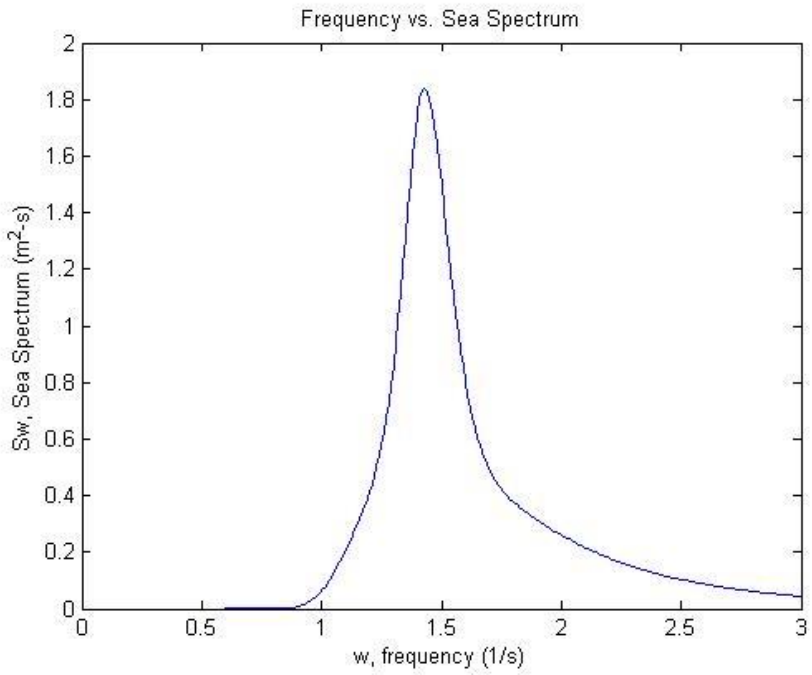

Figure 4.17: Frequency vs. Sea Spectrum.

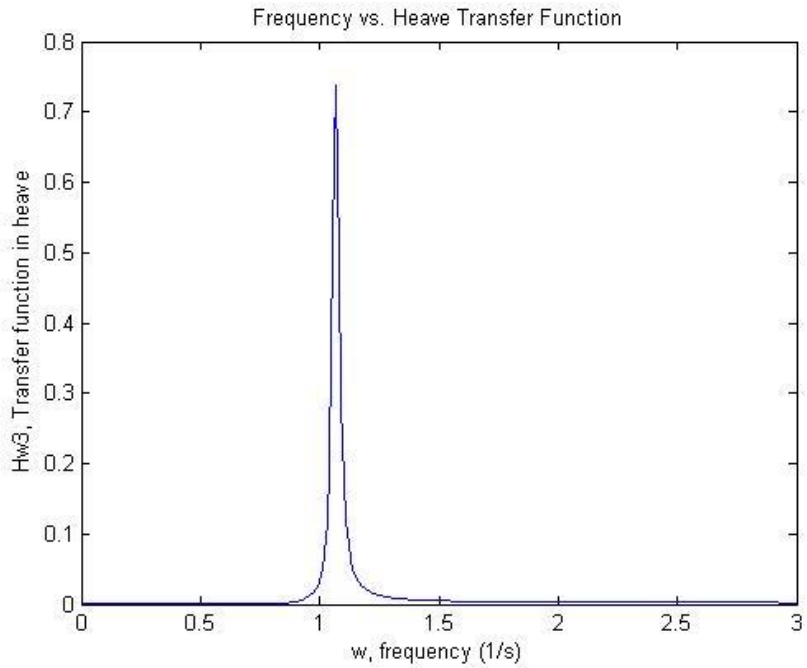

Figure 4.18: Frequency vs. Heave Transfer Function.

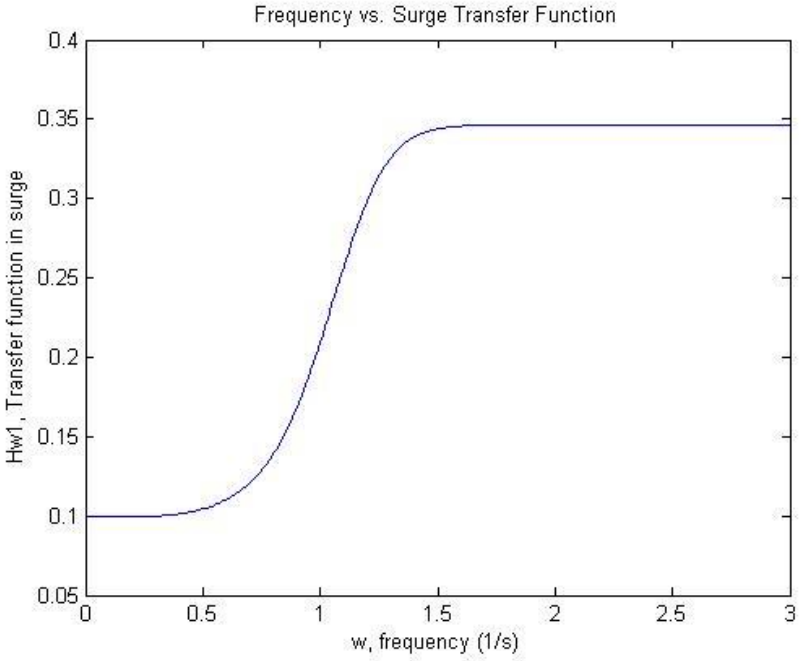

Figure 4.19: Frequency vs. Surge Transfer Function.

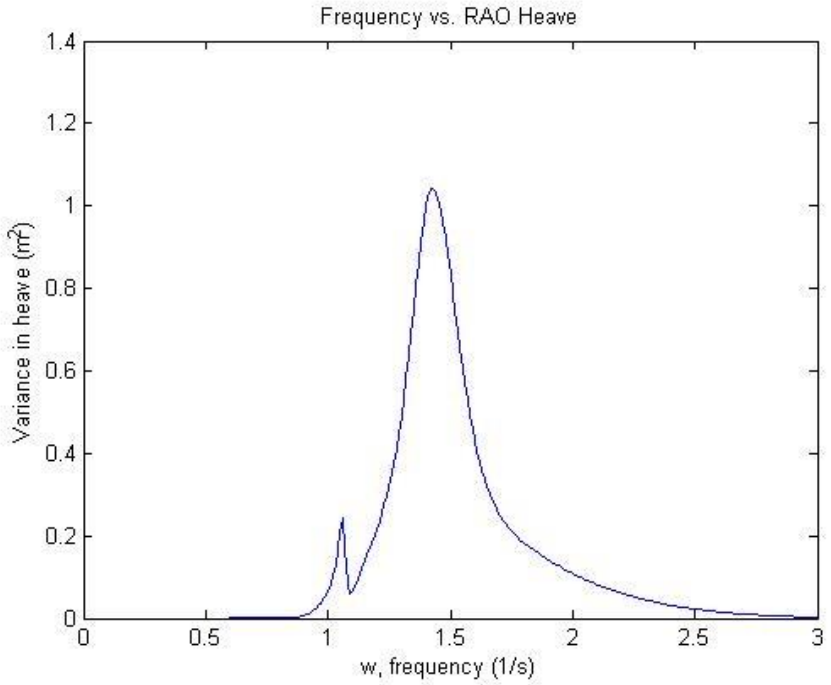

Figure 4.20: Frequency vs. RAO Heave.

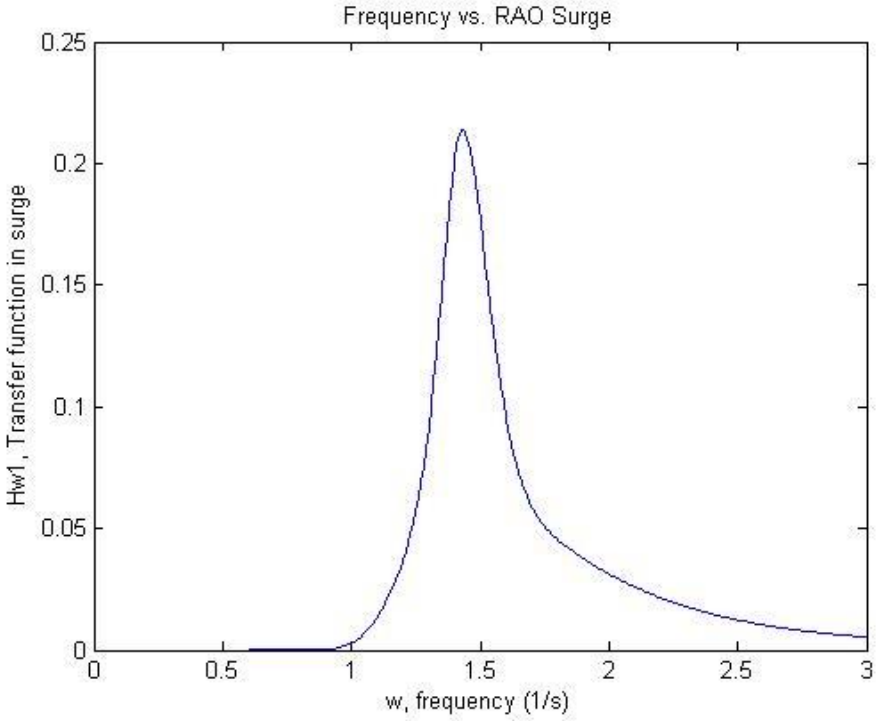

Figure 4.21: Frequency vs. RAO Surge.

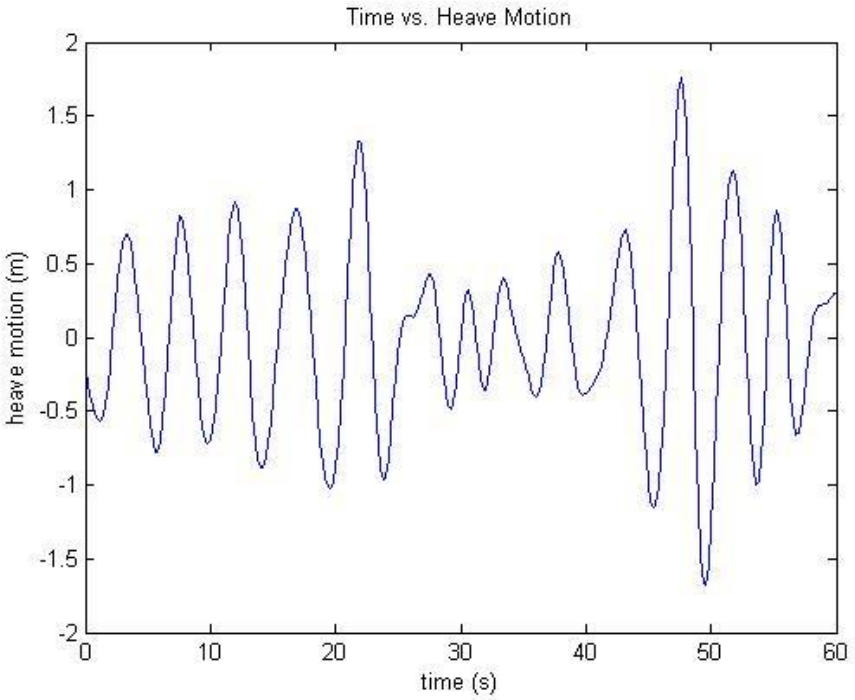

Figure 4.22: Time vs. Heave Motion.

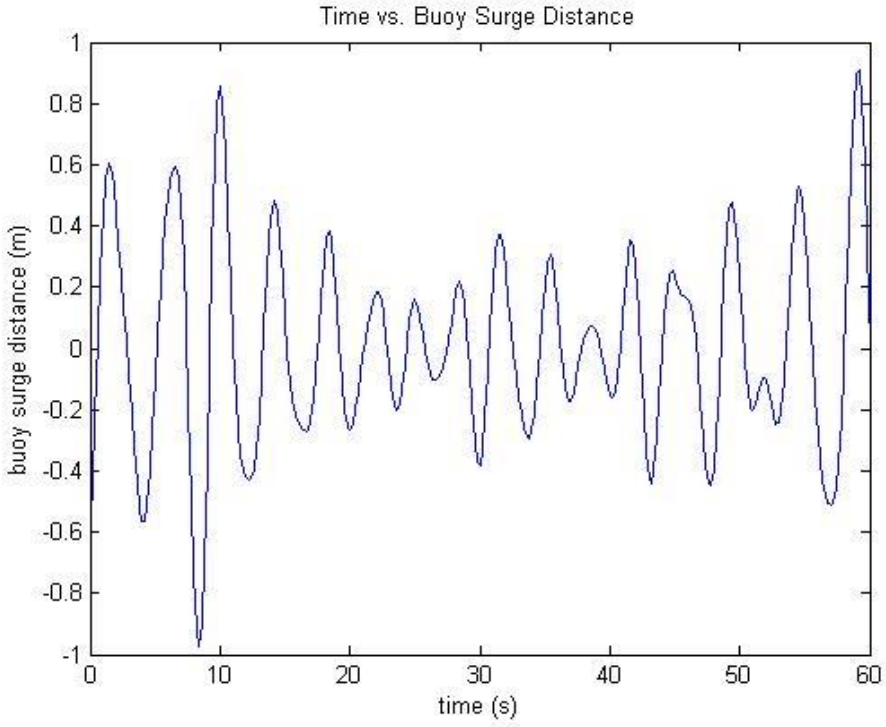

Figure 4.23: Time vs. Buoy Surge Distance.

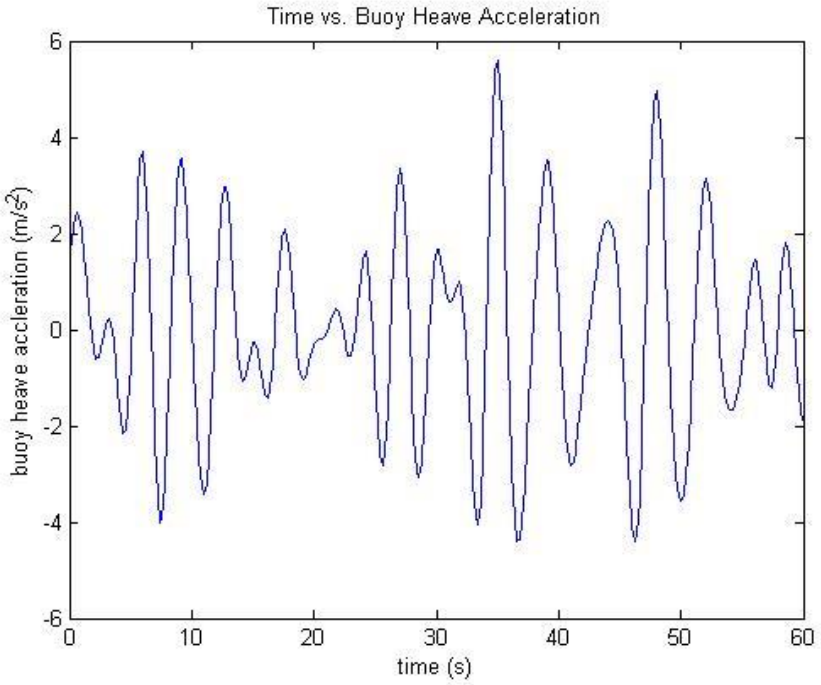

Figure 4.24: Time vs. Buoy Heave Acceleration.

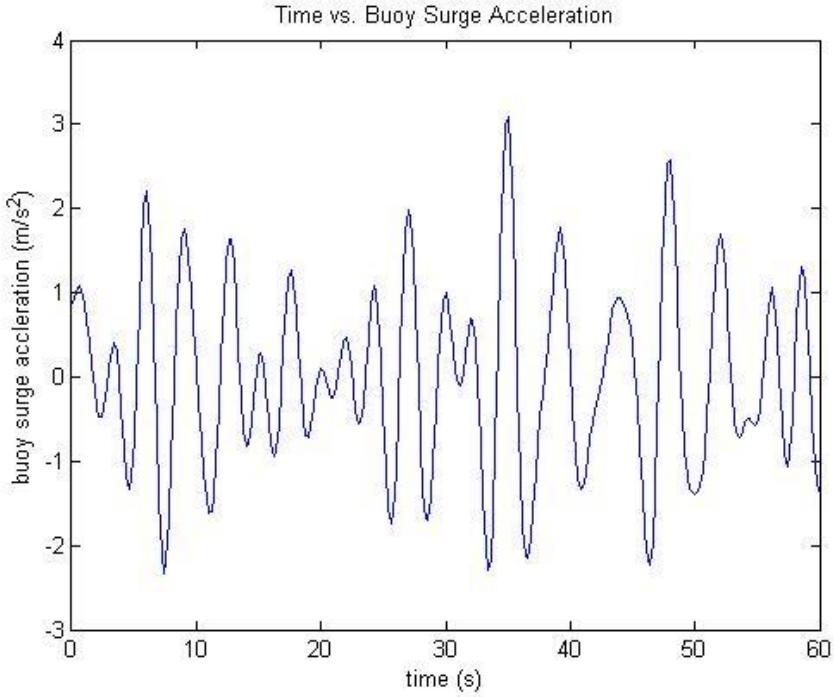

Figure 4.25: Time vs. Buoy Surge Acceleration.

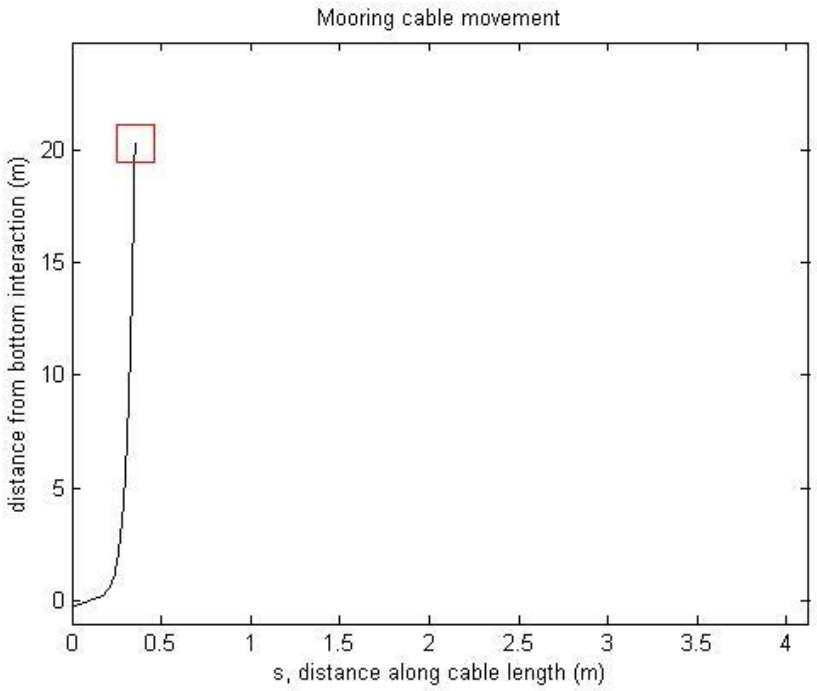

Figure 4.26: Buoy modeled in MATLAB program.

It would be recommended to use this tool when placing a buoy using a chain mooring in a new location. This tool has shown that it is capable of predicting chain wear in a mooring, but it does not take into account some various environmental factors and makes many assumptions. First, this program assumes the geometry is a floating cylinder; actual geometry would need to be implemented into the program to yield more accurate results. The program does not take into account different bottom types; therefore if the buoy is placed on coral or rock, the chain wear calculation will not be conservative. One last thing this program does not take into account is the coupling effect of all six degrees of freedom on the buoy and how it will affect the motion of the chain.

The time duration at which the testing was limited is due to the equipment shortcomings. Materials provided for this experiment were found among scrap piles within the URI Laboratory, with exception to the motor and controller used for the second test. Many of the moving parts had bearing surfaces that created much friction and often caused the grease to liquefy; the vertical slide used a guide with plastic ball bearings that were not exactly designed for the well over 200,000 cycles performed during this experiment, but worked without failure to provide satisfactory results when used. Each experiment was monitored during its entirety.

CHAPTER 5

CONCLUSIONS

This study provides a solid foundation for a program that will determine the chain wear of a buoy affixed to the seabed through use of a catenary system. It does give a general idea of what type of interlink wear rates to expect.

5.1 Contributions of Study

As a result of this study, just about any buoy with a chain mooring can be modeled and interlink wear can be determined given localized wave data long with characteristics of the buoy mooring system. The Coast Guard can use this model to optimize each buoy mooring by not only cutting out the excess chain but also run the model with different materials to see the affect it will have on chain wear. MOORSEL currently only provides mooring designs without testing the design for chain wear rate; it works well but the source code needs to be updated to operate within modern computer operating systems. This model can be implemented into MOORSEL's source code to yield chain wear results for each buoy, further optimizing the buoy design output of MOORSEL. The study can be used to predict chain wear in a catenary system in just about any application such as ships at anchor or mooring of floating piers.

5.1 Future Work

Future work for this study would include the addition of different geometries that would represent actual buoy shapes. With the formulas used, there would need to be experiments completed for each buoy geometry desired. These experiments would consist of determining the added mass and damping coefficients for heave and surge as a function of frequency. This task could be completed with advanced computational programs such as WAMIT. Within this experiment, it would also be recommended that the drag coefficient for this geometry be computed as well how the drag force affects the vertical orientation of the buoy when the buoy tension is anchored at the bridal connection points. One could also look into the sway degree of freedom or even all six degrees of freedom.

With the wear portion of the system, future work would include determining a wear solution using a non-Hertizan solution such as the Johnson-Kendall-Roberts (JKR) solution that assumes the contact is adhesive and validates the non-adhesive assumption made by Hertz. Another point of future work is to take the crossing cylinder assumption and bend it into chain geometry; in this case the contact will only be a circular point contact when both pieces first make tractions upon each other. The resultant will be wear shapes that may be non-circular in shape which may help yield more accurate wear measurements within the link of the chain. A very important piece of catenary chain wear that was not looked at is the wear rate on different bottom types as the chain slides along the bottom of the sea bed. With this research, one would need to place the problem into a three dimensional system and determine how the chain slides across the bottom if the buoy is oscillating or tidal and wind changes.

A.1 MATLAB Code

```
clear all

%function [w,Sw,Hw3,Hw1] =
RAO_cylinder(rho_w,g,b,aw,D,d,Ab,Lw,Delta,U,C,low_wave_frequency,wave
_frequency_interval,high_wave_frequency);

% Generate RAO for cylindrical buoy in irregular seas
% Jon Benvenuto and Jason Dahl, 1/14/2014

%************For editing purposes only
rho_w = 1025; %Density of seawater, kg/m^3
g = 9.81; %gravity constant, m/s^2
b = 2.44; %buoy radius, m
aw = 0.889; %wave amplitude, m ***took mean wave height from WIS
information***
D = 18.9; %depth of water, m
d = 2*b; %diameter of buoy, m
Ab = pi*b.^2; %buoy cross sectional area, m^2
Delta = 3856; %buoy displacement, kg
C = 25.02; %chain weight, kg/m
U = 0.01; %water current speed, m/s
low_wave_frequency = 0.01; %1/s
wave_frequency_interval = 0.01; %1/s
high_wave_frequency = 3; %1/s
t = 0:2:3600; %time, s
L = 47.2; %length of chain, m
di = 0.0381; %diameter of mooring chain, m
rho_s = 7858;    % kg/m^3, density of steel
E = 200*10^9;    % Pa, modulus of elasticity of steel
mu = 0.29;        % Poisson's Ratio of steel
sigma_y = 250*10^6; %Pa, yield stress of steel
kv = 1.004*10^-6; %kinematic viscosity, m^2/s
H13 = 1.42; %significant wave height
%**********************For editing purposes only


Disp = Delta+C*D;
T = Disp/(rho_w*Ab);
w = low_wave_frequency:wave_frequency_interval:high_wave_frequency;
k = (w.^2)/g;
we = w+w.^2*U/g;
x33 = w.*(T/g).^(0.5);
x = -b:0.01:b;
f=w/(2*pi);
gam = 3.3;
T13 = 3.3*H13^0.63; %significant wave period (m) formula 3.6 Goda
Tp = T13/(1-0.132*(gam+0.2)^-0.559); %peak period
```

```
fp = 1/Tp; %peak frequency

for q = 1:length(w)

    %Heave Motion
%     a33(q) = (1.0084*x33(q).^4 - 5.6393*x33(q).^3 +
11.451*x33(q).^2 - 9.716*x33(q) + 3.4925)*rho_w*Ab;  %Bonfiglio,
Brizzolara, & Chryssostomidis
%     b33(q) = (-0.4081*x33(q).^4 + 2.3098*x33(q).^3 -
4.4517*x33(q).^2 + 2.9483*x33(q) - 0.003)*rho_w*Ab.*x33(q);
%Bonfiglio, Brizzolara, & Chryssostomidis
    if d/T <= 2
        a33(q) = (0.8121.*x33(q).^4-
3.789.*x33(q).^3+6.4522.*x33(q).^2-
4.5569.*x33(q)+1.5133)*rho_w.*d.^2;
        b33(q) = (-1.1617.*x33(q).^4 + 3.4001.*x33(q).^3 -
2.5926.*x33(q).^2 - 0.5955.*x33(q) + 1.003).*rho_w.*d.^2.*w(q);
    elseif 4 <= d/T > 2
        a33(q) = (0.8968.*x33(q).^4 - 3.9503.*x33(q).^3 +
6.2816.*x33(q).^2 - 4.0893.*x33(q) + 1.2739).*rho_w.*d.^2;
        b33(q) = (0.7551.*x33(q).^2 - 1.7539.*x33(q) +
1.023).*rho_w.*d.^2.*w(q);
    elseif d/T > 4
        a33(q) = (0.8496.*x33(q).^4 - 3.6679.*x33(q).^3 +
5.6475.*x33(q).^2 - 3.5029.*x33(q) + 1.0653).*rho_w.*d.^2;
        b33(q)= (-1.31898.*x33(q).^4 + 2.5068.*x33(q).^3 -
0.3524.*x33(q).^2 - 1.8267.*x33(q) + 0.9999).*rho_w.*d.^2.*w(q);
    end
    c33(q) = rho_w*g*d;

    for n = 1:length(x)
        Gf33(n) = aw.*real(exp(1i.*k(q).*x(n))).*exp(-
k(q).*T).*(c33(q)-w(q).*(we(q).*a33(q)-1i.*b33(q))); %excitation
force in heave, PNA, Vol III, P.44
    end
    Gf3(q) = trapz(x,Gf33);
    B33(q) = trapz(x,b33(q)*ones(size(x))); %Heave Damping
    A33(q) = trapz(x,a33(q)*ones(size(x))); %Heave Added Mass
    C33(q) = trapz(x,c33(q)*ones(size(x))); %Heave Restoring Force
    Hw3(q) = (Gf3(q)./(-
((Disp+A33(q)).*we(q).^2)+1i*we(q).*B33(q)+C33(q))); %Transfer
function in heave, PNA Vol III, P.43, eqn 99

    %Surge Motion

    Di = ((D/2)*(1+(sinh(2.*k(q)*D)./(2.*k(q)*D))));
    di = (sinh(k(q)*D)/(k(q)*Di));
    Y =
pi*(k(q)*di^2/(k(q)*b)^2)*((besselh(1,1,k(q)*b)/(besselh(0,1,k(q)*b)-
besselh(2,1,k(q)*b)))); % Rahman and Bhatta, 1993
    A11(q) = -real(Y)*rho_w.*b.^3;
    B11(q) = -imag(Y)*rho_w.*b.^3.*w(q);
    Gf11 = -((2*pi*1i*rho_w*g*aw*b./k(q)).*(besselj(1,k(q)*b)-
(besselj(0,k(q)*b)-
besselj(2,k(q)*b))).*(besselh(1,1,k(q)*b)./(besselh(0,1,k(q)*b)-
```

```
besselh(2,1,k(q)*b))).*(1-exp(-k(q)*T)));%excitation force in surge
(Finnegan, Meere and Goggins)
    Hw1 = real(Gf11./(-(Delta+A11).*w(q).^2)+1i.*w(q).*B11);
%transfer function in surge

    %Wave Motion
    if f(q) > fp
        sig = 0.09;
    else
        sig = 0.07;
    end

    Bj = (0.0624/(0.230+0.0336.*gam-0.185.*(1.9+gam)^-1))*(1.094-
0.01915*log(gam));
    Sw(q) = Bj.*H13.^2.*Tp.^-4.*f(q).^-5.*exp(-1.25.*(Tp.*f(q)).^-
4).*gam.^exp(-(Tp.*f(q)-1).^2/(2.*sig.^2));
end
figure(1);
plot(w, Sw);

figure(2);
plot(w,Hw3);

figure(3);
plot(w,Sw.*abs(Hw3).^2);

figure(4);
plot(w,Hw1);

figure(5);
plot(w,Sw.*abs(Hw1).^2);

save('RAO_variables.mat','w','Sw','Hw3','Hw1');
%end
```

```
% Calculate time history for buoy response and waves
% Jon Benvenuto and Jason Dahl 1/14/2014

%function [R3,W,R1,t,Buoy_accel1]=RAO_time(t);
clear all;

%************For editing purposes only
rho_w = 1025; %Density of seawater, kg/m^3
g = 9.81; %gravity constant, m/s^2
b = 2.44; %buoy radius, m
aw = 0.889; %wave amplitude, m ***took mean wave height from WIS
information***
D = 18.9; %depth of water, m
d = 2*b; %diameter of buoy, m
Ab = pi*b.^2; %buoy cross sectional area, m^2
Delta = 3856; %buoy displacement, kg
C = 25.02; %chain weight, kg/m
U = 0.01; %water current speed, m/s
low_wave_frequency = 0.01; %1/s
```

```
wave_frequency_interval = 0.01; %1/s
high_wave_frequency = 3; %1/s
t = 0:2:3600; %time, s
L = 47.2; %length of chain, m
di = 0.0381; %diameter of mooring chain, m
rho_s = 7858;   % kg/m^3, density of steel
E = 200*10^9;   % Pa, modulus of elasticity of steel
mu = 0.29;       % Poisson's Ratio of steel
sigma_y = 250*10^6; %Pa, yield stress of steel
kv = 1.004*10^-6; %kinematic viscosity, m^2/s
H13 = 1.42; %significant wave height
%**********************For editing purposes only

load RAO_variables.mat

RAO1 = Sw.*abs(Hw1).^2;
RAO3 = Sw.*abs(Hw3).^2;

R1 = zeros(size(t));
R3 = zeros(size(t));
W = zeros(size(t));

for n = 1:length(w)-1
    wave_var(n) = trapz(w(n:n+1), Sw(n:n+1));
    RAO_var3(n) = trapz(w(n:n+1), RAO3(n:n+1));
    RAO_var1(n) = trapz(w(n:n+1), RAO1(n:n+1));
    w_avg(n) = (w(n)+w(n+1))/2;
    phi = rand(1)*2*pi;
    R1 = R1 + sqrt(2)*sqrt(RAO_var1(n))*cos(w_avg(n)*t + phi);
    R3 = R3 + sqrt(2)*sqrt(RAO_var3(n))*cos(w_avg(n)*t + phi);
    W = W + sqrt(2)*sqrt(wave_var(n))*cos(w_avg(n)*t + phi);
end

Buoy_vel1 = 1/(mean(diff(t)))*cdiff(R1);
Buoy_accel1 = 1/(mean(diff(t)))*cdiff(Buoy_vel1);
Buoy_vel3 = 1/(mean(diff(t)))*cdiff(R3);
Buoy_accel3 = 1/(mean(diff(t)))*cdiff(Buoy_vel3);

save('WearRateInputs.mat','R3','W','R1','t','Buoy_accel1');

figure(1)
plot(t,R3);

figure(2)
plot(t,W);

figure(3)
plot(t,Buoy_vel3);

figure(4)
plot(t,Buoy_vel1);

figure(5)
plot(t,R1);
```

```
%end
```

```
clear all;
load WearRateInputs.mat

%************For editing purposes only
rho_w = 1025; %Density of seawater, kg/m^3
g = 9.81; %gravity constant, m/s^2
b = 2.44; %buoy radius, m
aw = 0.889; %wave amplitude, m ***took mean wave height from WIS
information***
D = 18.9; %depth of water, m
d = 2*b; %diameter of buoy, m
Ab = pi*b.^2; %buoy cross sectional area, m^2
Delta = 3856; %buoy displacement, kg
C = 25.02; %chain weight, kg/m
U = 0.01; %water current speed, m/s
low_wave_frequency = 0.01; %1/s
wave_frequency_interval = 0.01; %1/s
high_wave_frequency = 3; %1/s
t = 0:2:3600; %time, s
L = 47.2; %length of chain, m
di = 0.0381; %diameter of mooring chain, m
rho_s = 7858;    % kg/m^3, density of steel
E = 200*10^9;    % Pa, modulus of elasticity of steel
mu = 0.29;        % Poisson's Ratio of steel
sigma_y = 250*10^6; %Pa, yield stress of steel
kv = 1.004*10^-6; %kinematic viscosity, m^2/s
H13 = 1.42; %significant wave height
%**********************For editing purposes only


awc = 3.02;  %kg/m, average weight of 0.5 inch chain
phi_last = 0;
WearVol_total = 0;

% Steady State Current Analysis
T = Delta/(rho_w*Ab);

Renyolds_num = U*2*b/kv;
    %coefficient of drag of a cylinder, horizontal flow
    if Renyolds_num < 200000
        Cd = 0.0343*log(Renyolds_num)+0.6861;
    elseif 500000 < Renyolds_num > 200000
        Cd = -0.735*log(Renyolds_num)+9.936;
    else
        Cd = 0.1796*log(Renyolds_num)-2.1026;
    end
CurrentForce = Cd*0.5*rho_w*(U^2)*2*b*T; %N, force of the current
L = 90; %length of chain, m
```

```
for n=1:length(t);

s = 0:L/10:L;       %m, distance along cable
H_buoy(n) = CurrentForce+Buoy_accel1(n).*Delta; % N, Max horizontal
force on bouy from ocean currents
De(n) = D+R3(n);         % m, depth of water w/wave

A = awc/rho_s;     % m^2, average cross-sectional area of chain
a = pi*(di/2).^2;   % area of one side of chain link

% I also assume that the cable is not extremely taut and therefore
its extension
% can be ignored.

w0 = awc*g;       % N/m, effective weight per unit length before
stretching

V_buoy(n) =
real(w0.*L/2+(w0.*De(n)/2).*(1+(4*H_buoy(n).^2)./(w0.^2.*(L^2-
De(n).^2))).^0.5); % N, vertical force at buoy

Te = (H_buoy(n).^2+(V_buoy(n)-w0.*(L-s)).^2).^0.5;  % N, Effective
tension in line
for y = 1:length(s)
    z(y) = ((H_buoy(n)./w0).*(sqrt(1+((V_buoy(n)-w0.*(L-
s(y)))./H_buoy(n)).^2)-sqrt(1+((V_buoy(n)-w0*L)./H_buoy(n)).^2))); %
m, depth as a function of s
    x(y) = (H_buoy(n)./w0).*(asinh((V_buoy(n)-w0.*(L-
s(y)))./H_buoy(n))-asinh((V_buoy(n)-w0*L)./H_buoy(n)));   % m,
horizontal distance as function of s

    if z(y) < 0
        L = L - 0.5;
    elseif L < D
        L = D;
    end

end

phi = atan((V_buoy(n)./H_buoy(n)-(w0./H_buoy(n)).*(L-s))); %(Jensen
2010, p. 56) rad, angle of midline of cable
phi_diff = abs(phi-phi_last);
sd = phi_diff*di/2; %Sliding Distance (m) = radius of chain
link*change in phi
H = Te.*cos(phi);                                % N, horizontal force
V = Te.*sin(phi);
K = 0.00520; %Dimensionless Wear Rate (from experiemtns)
H = 183*10^6; %Material Hardness (1022 steel)

WearVol = (K.*Te.*sd)./H;
WearVol_total = WearVol+WearVol_total;
phi_last = phi;
```

```
 figure(1)
 plot(x,z,'k',x(end),z(end),'rs','MarkerSize',20)
 axis([0 D*1.5 -20 L])



end

%commands to write a video of plot
% writerObj = VideoWriter('sample.avi'); % Name
% writerObj.FrameRate = 60; % How many frames per second.
% open(writerObj);
%insert 'for loop' with plot
%close(writerObj);

figure(2)
plot(s,phi);

figure(3)
plot(s,WearVol_total);

%Longitivity Calculation

Vol = max(WearVol_total)/2;
r = di/2;
dd = di-real(((sqrt(3).*sqrt(3.*Vol.^2-4*pi.*r.^3.*Vol)+2*pi.*r.^3-
3*Vol).^(1/3))./((2*pi).^(1/3))+((r.^2).*(2*pi).^(1/3))./((sqrt(3).*s
qrt(3.*Vol.^2-4*pi.*r.^3.*Vol)+2*pi.*r.^3-3.*Vol).^(1/3))); %Volume
of spherical cap, Wikipedia
WearDia = (di-dd)/2+r;
WearDiain = WearDia*39.37; % inches, final worn diameter of chain
a = sqrt(-dd*(dd-2*r));
thetap = acos(1-(2*a^2/r^2));
Aremaining_sqin = (r^2/2)*(thetap-sin(thetap))*1550;
TSY = 34100; %psi, tensile strength yeild
TSU = 61600; %psi, tensile strength ultimate
Yeild = Aremaining_sqin*TSY; %Yeild Force, pounds
Break = Aremaining_sqin*TSU; %Break Force, pounds

%end
```

Appendix A.2: U.S. Coast Guard Specification 121032 Rev H

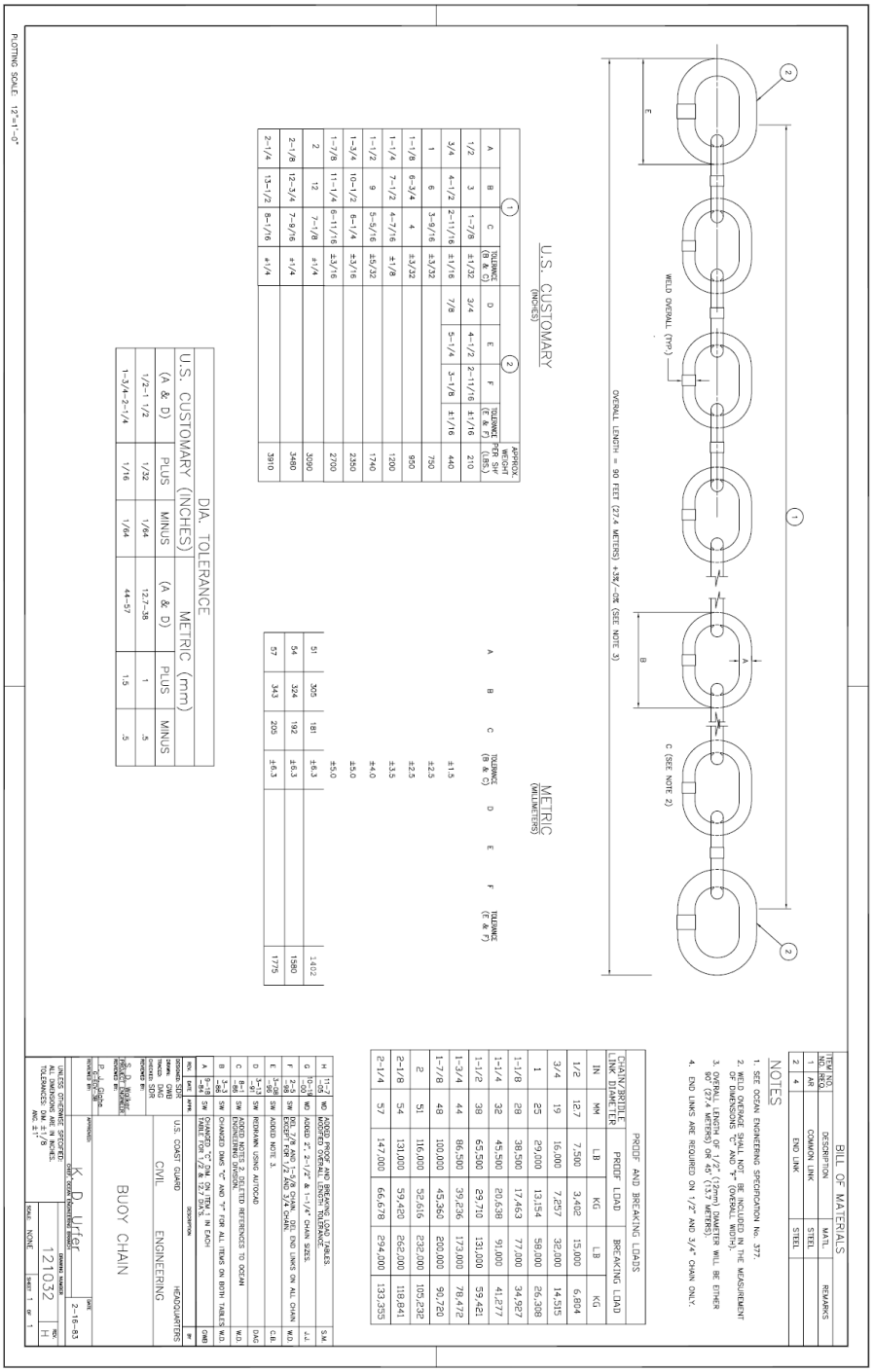

Appendix A.3: U.S. Coast Guard Chain Dimensions (USCG, 2010)

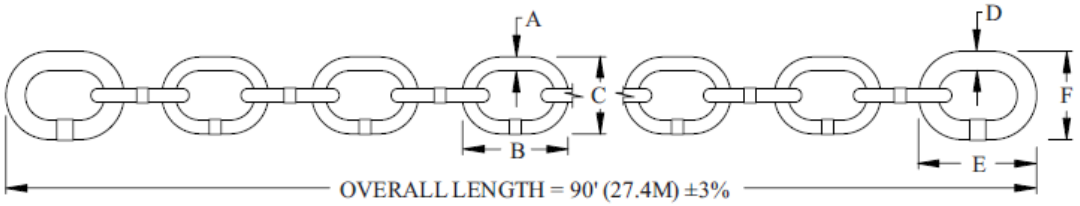

DIMENSIONS (INCHES)						PHYSICAL VALUES				
COMMON LINKS			END LINKS*			PROOF	BREAK	WEIGHT		DRY SHOT
A	B	C	D	E	F	LOAD	LOAD	(LBS/FT)	DRY	WEIGHT (LBS)
1/2	3	1-7/8	3/4	4-1/2	2-11/16	7,500	15,000	2.33	2.03	210
3/4	4-1/2	2-11/16	7/8	5-1/4	3-1/8	16,000	32,000	4.88	4.24	440
7/8**	5-1/4	3-1/8	1-1/8	6-3/4	4	22,000	44,000	6.61	5.75	595
1	6	3-9/16	1-1/4	7-1/2	4-7/16	29,000	58,000	8.33	7.24	750
1-1/8	6-3/4	4	1-1/4	7-1/2	4-7/16	38,500	77,000	10.55	9.17	950
1-1/4	7-1/2	4-7/16	1-1/2	9	5-5/16	45,500	91,000	13.33	11.59	1,200
1-1/2	9	5-5/16	1-7/8	11-1/4	6-11/16	65,500	131,000	19.33	16.8	1,740
1-5/8**	9-3/4	5-13/16	1-7/8	11-1/4	6-11/16	76,500	163,000	22.52	19.59	2,027
1-3/4	10-1/2	6-1/4	2-1/8	12-3/4	7-7/16	86,500	173,000	26.11	22.70	2,350
1-7/8	11-1/4	6-11/16	2-1/8	12-3/4	7-7/16	100,000	200,000	30.00	26.08	2,700
2	12	7-1/8				116,000	232,000	34.33	29.85	3,090
2-1/8	12-3/4	7-9/16				131,000	262,000	38.66	33.62	3,480
2-1/4	13-1/2	8-1/16				147,000	294,000	43.44	37.78	3,910

Appendix A.4: U.S. Coast Guard Chain Minimum Wear Chart (USCG, 2010)

Buoy Type	Recommended Mooring Chain				Minimum Wear Measurement
9X35LWR	1-7/8″	1-3/4″	1-5/8″	1-1/2″	1-1/16″
9X32LR	1-7/8″	1-3/4″	1-5/8″	1-1/2″	1-1/16″
9X20R	1-3/4″	1-1/2″	1-1/4″		7/8″
8X26LR	1-3/4″	1-1/2″	1-1/4″		7/8″
8X26LWR	1-1/2″	1-1/4″			7/8″
8X21LR	1-3/4″	1-1/2″	1-1/4″	1-1/8″	25/32″
7X20LI	Use existing Mooring from Permanent Buoy				
7X17LR	1-1/2″	1-1/4″	1-1/8″	1″	25/32″
6X20LR	1-1/2″	1-1/4″	1-1/8″	1″	25/32″
5X11LR	1-1/4″	1-1/8″	1″		25/32″
5X9LFR	1″	7/8″	3/4″		1/2″
3.5X8LR	1″	7/8″	3/4″		1/2″
1CR/1NR	1-1/2″	1-1/4″	1-1/8″		25/32″
2CR/2NR	1-1/4″	1-1/8″	1″	7/8″	25/32″
3CR/3NR	1″	7/8″	3/4″		1/2″
3CI/3NI	1″	7/8″	3/4″		1/2″
5CR/5NR	1/2″				11/32″
5CI/5NI	1/2″				11/32″
2CFR/2NFR	1-1/8″	1″	7/8″	3/4″	1/2″
3CFR/3NFR	7/8″	3/4″	1/2″		11/32″
4CFR/4NFR	3/4″	1/2″			11/32″
5CFR/5NFR	1/2″				11/32″
6CFR/6NFR	1/2″				11/32″
FWCFR/FWNFR	1/2″				11/32″
5CPR/5NPR	1/2″				11/32″

Appendix A.5: U.S. Coast Guard Characteristics of Buoys (USCG, 2010)

3.d.

PHYSICAL CHARACTERISTICS OF STANDARD LIGHTED BUOYS*

Characteristics \ Buoy Type	9X35 LWR	9X32 LR	9X20 B/GR	8X26 LR	8X26 LWR	8X21 LR	7X20 LI	7X17 LR	6X20 LR	5X11 LR	5X9 LFR	3.5X8 LR
BUOY WEIGHT (LB)	18,500	17,500	8,000	11,800	12,100	13,900	6,500	7,800	6,500	3,000	1,500	1,500
FLOODED WEIGHT (LB)	52,000	53,000	24,000	34,000	33,000	33,000	19,000	24,500	17,000	9,000	—	4,000
BUOY DRAFT (FT-IN)	15-10	11-7	5-4	10-4	10-5	7-9	10-7	5-6	9-0	3-9	2-9	2-9
FREEBOARD (FT-IN)	3-0	4-7	2-6	3-1	3-0	2-3	3-1	3-0	2-1	2-1	1-1	1-4
BRIDLE SIZE CHAIN DIA X LENGTH (IN X FT)	1-1/2 20	1-1/2 18	1-1/4 15	1-1/4 15	1-1/4 15	1-1/4 15	1-1/4 15	1-1/4 15	1 12	1 12	—	7/8 10
MOORING CHAIN SIZE (IN)	SEE TABLE 2-12											
SINKER SIZE (LB)	12,750	12,750	8,500	8,500	8,500	8,500	* *	8,500	5,000	4,000	4,000	3,000

Appendix A.5: U.S. Coast Guard Characteristics of Buoys (USCG, 2010)

PHYSICAL CHARACTERISTICS OF STANDARD FOAM AND PLASTIC UNLIGHTED BUOYS

Characteristics \ Bouy Type	2 CFR	2 NFR	3 CFR	3 NFR	4 CFR	4 NFR	5 CFR	5 NFR	6 CFR	6 NFR	FW CFR	FW NFR	5 CPR	5 NPR
BUOY WEIGHT (LB)	1,100	1,025	525	500	195	180	115	115	65	65	200	195	114	114
BUOY DRAFT (FT-IN)	5-3	5-3	3-1	3-1	2-10	2-10	3-0	3-0	2-4	2-4	1-1	1-1	3-6	3-6
FREEBOARD (FT-IN)	2-0	2-0	1-4	1-4	0-11	0-11	0-10	0-10	1-11	1-11	1-0	1-0	3-0	3-0
MOORING CHAIN SIZE (IN)	SEE TABLE 2-12													
SINKER SIZE (LB)	3,000	3,000	2,000	2,000	1,000	1,000	500	500	500	500	1000+	1000+	500	500

Appendix A.5: U.S. Coast Guard Characteristics of Buoys (USCG, 2010)

PHYSICAL CHARACTERISTICS OF STANDARD UNLIGHTED STEEL BUOYS

Buoy Type / Characteristics	1 CR	1 NR	2 CR	2 NR	3 CR	3 NR	5 CR	5 NR	3 CI	3 NI	5 CI	5 NI	4 CR	4 NR	6 CR	6 NR	6 CT	6 NT
BUOY WEIGHT (LB)	6,100	6,000	2,800	2,600	1,200	1,175	710	710	1,550	1,550	700	700	465	470	160	165	165	170
FLOODED WEIGHT (LB)	18,500	18,400	8,400	8,300	3,200	3,200	1,800	1,800	4,200	4,200	1,900	1,900	------	------	-----	-----	-----	-----
BUOY DRAFT (FT-IN)	8-7	8-4	6-3	6-1	4-4	4-4	5-1	5-1	7-7	7-7	5-0	5-0	5-0	5-0	3-10	3-10	4-0	4-0
FREEBOARD (FT-IN)	5-5	5-8	3-9	3-11	2-4	2-4	2-3	2-3	5-5	6-5	3-2	4-2	2-11	2-11	2-5	2-5	2-9	4-2
MOORING CHAIN SIZE (IN)	SEE TABLE 2-12												1/2*	1/2*	1/2*	1/2*	1/2*	1/2*
SINKER SIZE (LB)	8,500	8,500	4,000	4,000	3,000	3,000	2,000	2,000	3,000	3,000	2,000	2,000	2,000	2,000	500	500	500	500

Appendix A.6: U.S. Coast Guard Buoy Data from USCGC FRANK DREW off the coast of Virginia Beach, VA.

Chesapeake Bay Southern Approach Lighted Buoy 12

LLNR 470
DEPTH 58 FT
LENGTH: 135FT
CHAIN SIZE: 1 ½" (48/32")
BOTTOM TYPE: SAND
ACW: 7/32"
AP LATITUDE: **36-53-16.298N**
AP LONGITUDE: **075-53-07.343W**

Chesapeake Channel Lighted Buoy 4

LLNR **7050**
DEPTH 77 FT
LENGTH: 160FT
CHAIN SIZE: 1 ½" (48/32")
BOTTOM TYPE: MUD
ACW: 5/32"
AP LATITUDE: **36-57-48.911N**
AP LONGITUDE: **075-59-21.477W**

Thimble Shoal Channel Lighted Bell Buoy 1TS

LLNR **9205**
DEPTH: 62 FT
LENGTH: 155FT
CHAIN SIZE: 1 ½" (48/32")
BOTTOM TYPE: MUD
ACW: 4.6/32"
AP LATITUDE: **36-56-59.849N**
AP LONGITUDE: **076-01-25.049W**

BIBLIOGRAPHY

Bonfiglio, L., Brizzolara, S., & Chryssostomidis, C. (2012). Added Mass and Damping of Oscillating Bodies: a fully viscous numerical approach. *Recent Advances in Fluid Mechanics, Heat & Mass Transfer and Biology* (pp. 210-216). Cambridge: WSEAS Press.

Catalano, P., Wang, M., Iaccarino, G., & Moin, P. (2003). Numerical simulation of the flow around a circular cylinder at high Reynolds numbers. *Internation Journal of Heat and Fluid Flow*, 463-469.

Danzik, W. S. (1986). *Alloy Chain Validation.* Washington: U.S. Coast Guard.

Dinovitzer, A., Rene, J.-L., Silberhorn, R., & Steele, M. (1996). The Mooring Selection Guide (MSG) Software.

Faltinsen, O. M. (1990). *Sea Loads on Ships and Offshore Structures.* Cambridge: Cambridge University Press.

Finnegan, W., Meere, M., & Goggins, J. (2011). The Wave Excitation Forces on a Floating Vertical Cylinder in Water of Infinite Depth. *World Renewable Energy Congress* (pp. 2175-2182). Linkoping: Marine and Ocean Technology.

Ghadimi, P., Bandari, H. P., & Rostami, A. B. (2012). Determination of the Heave and Pitch Motions of a Floating Cylinder by Analytical Solution of its Diffraction Problem and Examination of the Effects of Geometric Parameters on its Dynamics in Regular Waves. *International Journal of applied Mathematical Research*, 611-633.

Goda, Y. (2010). *Random Seas and Dersign of Maritime Structures.* Yokohama: World Scientific.

Gutierrez-Miravete, E. (n.d.). *Chapter 6 Wear.* Retrieved March 18, 2014, from Friction and Wear of Materials: http://www.ewp.rpi.edu/hartford/~ernesto/F2012/FWM/Notes/ch06.html

Irvine, H. M. (1981). *Cable Structures.* Cambridge: The MIT Press.

Johnson, K. L. (1985). *Contact Mechanics.* Cambridge: Cambridge University Press.

Kohler, C. A. (1985). *Corrosive Wear of Alloy Steels for Buoy Chain.* Kingston: University of Rhode Island.

Lewis, E. V. (1989). *Principles of Naval Architectre.* Jersey City: The Society of Naval Architects and Marine Engineers.

Meng, H. C., & Ludema, K. C. (1995). Wear models and predicitive equations: their form and content. *Wear*, 443-457.

Mohs Hardness Scale. (n.d.). Retrieved Janurary 2014, 28, from Realgems.org: http://www.realgems.org/mohs.html

Newman, J. N. (1977). *Marine Hydrodynamics.* Cambridge: The MIT Press.

Paul, W., Irish, J., Gobat, J., & Grosenbaugh, M. (2007, March 19). *Coastal Mooring Design: Taught Elestomeric and Chain Caternary Surface Buoy Moorings.* Retrieved December 14, 2013, from WHOI: http://kelvin.whoi.edu/mooring.html

Pavani, R., & Ranghino, G. (1982). A Method to Compute the Volume of a Molecule. *Computers & Chemistry*, 133-135.

Popov, V. L. (2010). *Contact Mechanics and Friction.* Berlin: Springer-Verlag.

Ross, R. A. (1974). *An Experimental Determination of the Drag Coefficient of Buoy Mooring Chain.* Kingston: University of Rhode Island.

Segment of a Circle. (n.d.). Retrieved Janurary 24, 2014 , from Math Captain: http://www.mathcaptain.com/geometry/segment-of-a-circle.html

Spherical cap. (2011). Retrieved Feburary 11, 2014, from Wikipedia: http://en.wikipedia.org/wiki/Spherical_cap

Thompson, J. M., & Thompson, M. K. (2006). *A Proposal for the Calculation of Wear.* Cambridge: Massachusetts Institute of Technology.

USCG. (2010). *Aids to Navigation Manua-Technical, COMDTINST M16500.3A.* Washington, D.C.: U.S. Coast Guard.

Williams, J. A. (1999). Wear modelling: analytical, computational and mapping: a continuum mechanics approach. *Wear*, 225-229.